# Altered subcutaneous adipose tissue parameters after switching ART-controlled HIV+ patients to raltegravir/maraviroc

Jean-Philippe Bastard, Véronique Pelloux, Rohia Alili, Soraya Fellahi, Judith Aron-Wisnewsky, Emilie Capel, Bruno Fève, Lambert Assoumou, Edi Prifti, Christine Katlama, et al.

**Altered subcutaneous adipose tissue parameters after switching ART-controlled HIV+ patients to raltegravir/maraviroc**

Jean-Philippe BASTARD[1,2], Véronique PELLOUX[3,4], Rohia ALILI[3,4], Soraya FELLAHI[1], Judith ARON-WISNEWSKY[3,4], Emilie CAPEL[1], Bruno FÈVE[1,5], Lambert ASSOUMOU[6], Edi PRIFTI[7], Christine KATLAMA[6,8], Karine CLÉMENT[3,4], Jacqueline CAPEAU[1]

[1]Sorbonne Université, Inserm, Faculty of Medicine, Centre de Recherche Saint-Antoine (CRSA), ICAN, Paris, France

[2]Department of Biochemistry-Pharmacology-Molecular Biology, APHP, Henri-Mondor Hospital, Université Paris Est Créteil, France

[3] Sorbonne Université, Inserm, Faculty of Medicine, Nutrition and obesities: systemic approaches (NutriOmics), Paris, France

[4] Assistance Publique Hôpitaux de Paris, Sorbonne Université, Nutrition department, Pitié-Salpétrière hospital, CRNH Ile-de-France, GH APHP-Sorbonne Université, Paris, France

[5]Department of Endocrinology, CRMR Prisis, Saint-Antoine Hospital, GH APHP-Sorbonne Université, Paris France

[6] Sorbonne Université, Inserm, Faculty of Medicine, Institut Pierre Louis d'Epidémiologie et de Santé Publique (IPLESP), Paris, France

[7]IRD, Sorbonne University, UMMISCO, Bondy, France

[8]Department of Infectious Diseases, Pitié-Salpétrière hospital, GH APHP-Sorbonne Université, Paris France

Short title: fat alterations induced by RAL/MVC

Corresponding author and author to whom requests for reprints should be made:

Pr Jacqueline Capeau

Faculty of Medicine Sorbonne University, 27 rue Chaligny 75012 Paris France

e-mail: jacqueline.capeau@inserm.fr

**Conflict of interest and source of funding**

BF has received personal fees for lectures from Amgen, Sanofi, Lilly, Astra-Zeneca, Novo Nordisk

JC has received grants from ViiV healthcare and MSD, and personal fees for lectures from ViiV healthcare, MSD, Gilead, Janssen.

For the remaining authors none were declared

The ANRS 157 ROCnRAL study was sponsored and funded by the French National Institute for Health and Medical Research (INSERM)–French National Agency for Research on AIDS and Viral Hepatitis (ANRS); ViiV Healthcare (France) and Merck Sharp & Dohme (France) provided maraviroc and raltegravir, respectively, for this trial.

This study received a grant from ANRS. Support was also obtained by RHU CARMMA grant (ANR-15-RHUS-0003), the French National Agency of Research (ANR-Captor project), and ANR-10-IAHU-05 (IHU-ICAN) and FORCE (as part of F-Crin), as well as the Fondation pour la Recherche Médicale (FRM DEQ20120323701 and EQU201903007868).

**Abstract**

Objective: To evaluate the effect on anthropometric, metabolic and adipose tissue parameters of switching ART-controlled persons living with HIV (PLWH) from a protease-inhibitor regimen to raltegravir/maraviroc.

Design: Substudy of ROCnRAL-ANRS157 with investigation of subcutaneous abdominal adipose tissue (SCAT) biopsy at inclusion and study end.

Methods: We performed lipoaspiration of paired SCAT samples, histology on fresh/fixed samples and examined the transcriptomic profile analyzed using Illumina microarrays after RNA extraction. Statistical analyses used Wilcoxon-paired test.

Results: The patients (n=8) were mainly male (7/8), aged (mean±SEM) 54.9±1.2 years, BMI 26.1±1.2 kg/m$^2$, CD4: 699±56 cells/mm$^3$, all viral load (VL)<50 copies/mL. After a follow-up of 6±0.5 months, all PLWH remained with VL<50 copies/mL. BMI, trunk and limb fat amounts were unchanged yet systemic insulin resistance increased. Adipose tissue histology was unchanged except for borderline increased adipocyte diameter (*P*=0.1). Amongst the 16,094 RNA transcripts, 458 genes were up-regulated and 244 down-regulated. Analyses of the KEGG and GO databases, evaluating modifications in the main functional pathways, revealed that genes related to immune recognition/function were less expressed as were genes encoding T-cell receptor and receptor signaling pathways. The gene expression profiles indicated decreased

inflammation but genes involved in adipogenesis and insulin resistance were overexpressed.

Conclusion: After 6 months of raltegravir/maraviroc, adipogenesis-related gene profile was enhanced in SCAT, in agreement with a tendency for increased adipocyte size. Enhanced SCAT insulin resistance-related profile was concordant with higher systemic insulin resistance. However, immune activation/inflammation profile was globally lowered. We propose that raltegravir/maraviroc might favor SCAT gain but reduce inflammation/immune activation.

**Key words**

Subcutaneous adipose tissue, raltegravir, maraviroc, transcriptomics, histology, adipogenesis, inflammation/immune activation, insulin resistance

**Introduction**

Integrase strand transfer inhibitors (INSTI) are currently a highly recommended option in ART-naïve and also ART-experienced people living with HIV(PLWH) given their high and rapid efficacy and safe metabolic profile. However, some INSTIs (mainly dolutegravir and bictegravir but also raltegravir) have been recently associated with a global weight and fat mass gain[1]. Even if the mechanisms remain elusive, we have previously shown that some INSTIs induced adipocyte hypertrophy, adipose tissue (AT) fibrosis and insulin resistance[2]. However, in this previous work evaluating PLWH with severe obesity, we could only cross-compare AT samples issued from INSTI-treated or INSTI-untreated PLWH. The ROCnRAL study (Clinical-Trials.gov: NCT1420523), evaluated the efficacy of a dual therapy associating an INSTI, raltegravir, to the CCR5 inhibitor, maraviroc, in patients suppressed on a protease-inhibitor (PI)-containing regimen but was prematurely stopped due to insufficient virologic control[3]. Herein, we analyzed SCAT individual variation before and 6 months after raltegravir/maraviroc initiation.

Increased weight/fat has been reported in PLWH who received some PI-based treatment[1]. Due to PI-related increased risk of cardiometabolic diseases, aging PLWH have been often switched to an INSTI-based therapy due to the lipid-lowering effect of INSTI[4-6]. However, INSTI-related weight/fat gain also raises concern regarding increased cardiometabolic risk. This risk has not been yet clearly shown for cardiovascular diseases. Regarding insulin resistance and diabetes, results are discrepant[4, 7].

Otherwise, maraviroc has been associated with changes in immune profile and a favorable effect on cardiovascular parameters in PLWH[8, 9]. Moreover, maraviroc may exert anti-fibrotic effects on the liver[10, 11].

We performed a careful investigation of patients from the ROCnRAL study and examined the individual evolution of anthropometric, metabolic, inflammatory and AT parameters six months after initiation of the dual raltegravir/maraviroc therapy.

## Patients and methods

### Patients

Seventeen patients were enrolled into the ROCnRAL fat sub-study prior to study discontinuation. Eight had subcutaneous-AT (SCAT) biopsies both at initiation and end: they were aged (mean±SEM) 54.9±1.2 years at inclusion, 87% male, 87% Caucasian, 13% African, CD4 699±56 cells/$mm^3$, VL<50 copies/mL. They received raltegravir/maraviroc for a mean duration of 6±0.5 months.

### Systemic markers

Adiponectin, leptin and inflammatory markers (hsCRP, hsIL-6, sCD14, sCD163) were measured on stored serum samples by immunonephelometry or ELISA[12]. Insulin resistance was measured by the quantitative insulin sensitivity check index (QUICKI) = $1/[\log(G_b) + \log(I_b)]$ where $G_b$ is fasting plasma glucose (milligrams per deciliter), and $I_b$ is fasting plasma insulin (microunits per milliliter).

**Fat collection and histology**

Subcutaneous-AT(SCAT) samples were collected by a single operator (JPB) by needle lipoaspiration from the periumbilical area under local anesthesia.

Histology was analyzed on fresh tissue to evaluate adipocyte size/volume and on fixed tissue to evaluate fibrosis by Sirius Red staining (scored using arbitrary units 0-3)[13].

**mRNA extraction and transcriptomics**

Total RNA was extracted using a RNeasy total-RNA minikit (QIAGEN, Verlo, The Netherlands), quality/concentration assessed (Agilent-2100 bioanalyzer, Agilent-Technologies, Santa-Clara, USA) and biotin-labeled complementary-RNA obtained (Ambion, Thermo-Fischer-Scientific, Waltham, USA). Hybridization processes used Illumina human HT-12 version-4.0 Expression BeadChips (Illumina-Inc, San-Diego, USA). Probes were detected using an Illumina-BeadArray Reader[14].

Raw data were extracted using the numerical results (Illumina Genome-Studio 2011.1 software). The group comparisons used Student's *t* test. To estimate the false-discovery-rate, we filtered the resulting *P* values at 5% and used the Benjamini-Hochberg procedure[14]. In the 16 paired samples, 80% of genes had valid expression. The Significance Analysis of Microarrays (SAM), shown as a switch R plot, indicated the genes significantly up- and down-regulated after the switch (suppl Figure 1). An automated annotation procedure of the differentially expressed genes used the KEGG (Kyoto Encyclopedia of Genes and Genomes) or GO (Gene Ontology) annotation databases. Functional analyses used the FunNet package.

**Statistics**

The paired results were compared using Wilcoxon-test (significant *P*<5%, Prism and Statview software). Transcriptomics results were adjusted for multiple testing (significant q<5%, SAM package).

**Results**

All patients remained controlled (VL<50 copies/mL) with unmodified CD4 and CD8 levels (Table 1). BMI was unchanged after 6 months, as waist circumference, waist-to-hip ratio, trunk and limb fat amounts. However, hip circumference increased from 94.9 to 99.1 cm (*P*=0.03). Regarding metabolic parameters, insulin increased (10.7 to 21.5 mU/L, p<0.05). To evaluate insulin resistance, we used QUICKI, better correlated to the gold standard euglycemic hyper-insulinemic clamp IS value than HOMA-IR[15]: QUICKY decreased from 0.342 to 0.315 (*P*<0.05), in favor of increased insulin resistance. The level of adiponectin and inflammatory/immune activation markers (hsCRP, hsIL-6, sCD14, sCD163) was unmodified but leptin tended to increase (*P*=0.08, Table 1).

Adipose tissue histology revealed that adipocyte diameter and volume increased yet not reaching significance (*P* =0.10). The level of parenchyma fibrosis remained unchanged.

Transcriptomic analysis performed in the 16 paired samples identified 16,094 expressed RNA transcripts: 244 genes were down-regulated with a fold-change of 0.66 to 0.9 and 458 genes up-regulated with a fold-change of 10.6 to 1.1 (supplemental Tables 1 and 2).

Using the GO database, the gene network (Fig 1) revealed globally increased DNA replication and transcription, suggesting AT remodeling. Importantly, T-cell receptor signaling pathway was down-regulated as were pathways related to viral infection. Using the KEGG annotation database (Suppl Fig 2), the most enriched function was ubiquitin-mediated proteolysis (19.4%) and the main impoverished function (29.7%) was related to ribosomes involved in protein synthesis, indicating major switch-induced protein remodeling. Functions related to immune cell recognition and immune-related diseases were down-regulated.

Among the individual down- and up-regulated genes, we selected those with the larger amplitude of variation (less than x0.8 or more than x3). Two main categories were affected: *i)* genes expressed in immune cells and involved into T-cell and macrophage activation, and *ii)* genes involved into adipogenesis and insulin sensitivity in adipocytes. Among down-regulated immune-related genes, several encode proteins from the TCR superfamily: CD247 x0.7, TNFRSF4 (tumor-necrosis-factor receptor superfamily member-4) x0.7, CD3D (CD3 molecule$\delta$ in the CD3-TCR complex) x0.7. Other genes encode proteins expressed in T-cells: IL7R x0.7 and GIMAP4 (GTPase, IMAP-family-member-4) x0.7 in the IL7R pathway, GZMB (granzyme B) x0.7, CD58 x0.8, SEMA4D (semaphoring-4D) x0.8, in favor of a decreased level of T-lymphocytes within AT.

Several immune-related genes were upregulated as genes expressed in macrophages favoring the M2 versus M1 phenotype: DAB2/CD11b x4.7, FOXO3 (forkhead-box-O3) x3.9, TCF4 (transcription factor-4) x3.6, CREB1 (cAMP-responsive-element-binding-protein-1) x3.5, IL10 x3.1. A number of genes were involved into decreased T-

lymphocyte immune activation: MAGT1 (magnesium transporter-1) x5.3, DAB2/CD11b x4.7, IL17RD (IL17 receptor-D) x4.0. Also, genes encoding proteins inhibiting NFκB and decreasing inflammation were up-regulated: CDKN2AIPNL (CDKN2A-interacting-protein-N-terminal-like) x7.7, DUSP19 (dual-specificity phosphatase-19) x5.6, KLF6 (Kruppel-like factor-6) x5.5, TRIM3 (tripartite-motif-containing-13) x3.3, while few genes were positively involved into inflammation as SEMA3E (semaphoring-3E) x4.9. Taken as a whole, the gene expression profile suggested decreased T-lymphocytes number/activation and a shift to a M2 macrophage phenotype together with increased expression of anti-inflammatory genes.

Otherwise, up-regulated expression was observed for genes involved into adipogenesis: KLF6 x5.5, QRFRR (polyglutamated RF-amide peptide receptor) x5.5, CREB1 x5.0, FOXO3 x3.9, TRIM13 x3.3, DLC1 (deleted-in-liver-cancer-1) x3.3, IL10 x3.1.

Also, several genes in the insulin signaling pathways involved into increased insulin resistance were up-regulated: SEMA3E x4.9, PIP5K2B (phosphatidylinositol-5-phosphate-4-kinase, typeIIβ) x3.7, IL10 x3.1, while LEPROT (leptin-receptor-overlapping-transcript) x5.4 is related to insulin signaling.

**Discussion**

We report here that ART-suppressed PLWH switched to raltegravir/maraviroc presented metabolic and adipose tissue modifications over six months. While BMI and fat mass did not change, hip circumference increased indicating fat redistribution. Likewise, insulin resistance, evaluated by fasting glycemia/insulin levels, increased. SCAT exhibited enhanced expression of genes associated with adipogenesis and insulin resistance.

Otherwise, expression of genes related to T-lymphocytes was reduced and the gene profile suggested a shift towards decreased AT inflammation and a M2 anti-inflammatory macrophage phenotype.

INSTI have been recently associated with a global fat mass gain. We previously reported increased adipogenesis induced by dolutegravir and raltegravir *in vitro* together with adipocyte hypertrophy in SCAT and visceral AT samples issued from INSTI-treated PLWH and macaques[2]. Our present results are in good accordance. The fact that the two main categories of modified genes are involved into protein degradation/synthesis enlightens the marked effect of ART *versus* HIV on fat. Indeed, only switching ART regimen, without CD4 or VL change, deeply affected AT. Previous *in vitro* studies indicated that maraviroc was neutral regarding adipocyte differentiation[16]. Thus, increased adipogenesis, suggested by the gene expression profile, and borderline increased adipocyte size might result from the effect of raltegravir.

Regarding inflammation, in accordance with our present results, we observed in SCAT samples from obese PLWH the absence of inflammation (macrophage infiltration with crown-like structures) in samples issued from INSTI-treated patients by contrast to non-INSTI PLWH and HIV-negative controls[17]. Interestingly, increased weight in INSTI-treated PLWH was associated with decreased VAT density suggesting a lower inflammation level[18]. Therefore, INSTI could reduce AT inflammation and immune activation. Maraviroc was previously shown to decrease inflammatory cytokine expression in cultured adipocytes[16] and macrophage recruitment in AT induced by a

high-fat diet in mice[19]. Thus, both raltegravir and maraviroc could explain the decreased expression of immune and inflammation-related genes.

Switching to raltegravir/maraviroc was associated with surrogate markers of systemic insulin resistance, probably ART-related. Indeed, BMI remained unmodified and increased hip circumference is generally associated with a favorable metabolic profile. Accordingly, the expression of genes involved in insulin resistance was enhanced in agreement with *in vitro* studies using raltegravir[2]. Since maraviroc has not been reported to affect insulin sensitivity in PLWH and in endothelial cells[20], it is reasonable to hypothesize that the gene profile favoring insulin resistance is related to raltegravir. Clinical studies report discrepant data. We recently reported increased insulin resistance in patients switching from a PI-based regimen to raltegravir-etravirine[21] while, in a similar context, authors concluded that raltegravir increased insulin sensitivity[4].

AT fibrosis adversely impacts metabolic parameters[22]. We did not observe any modification in the level of global fibrosis in SCAT and only a few genes which expression was modified were directly related to collagen remodeling. We previously reported increased fibrosis in SCAT of INSTI-treated severely obese PLWH[2]. However, maraviroc reduces fibrosis in the liver, and is now evaluated in that setting in clinical trials in PLWH with non-alcoholic-fatty-liver disease[10, 11]. It might also be anti-fibrotic on AT. Possibly, treatment with both raltegravir and maraviroc could be globally neutral regarding AT fibrosis.

Circulating levels of adipokines and cytokines remained unchanged but our study lacked potency. Clinical trials using raltegravir or dolutegravir report, or not, modification in the level of these markers[4, 5, 23]. Likewise, maraviroc markedly improved atherosclerotic progression in HIV-suppressed PLWH at high cardiovascular risk[8], but the beneficial effect on the arterial wall was local and not associated with decreased inflammatory systemic markers.

Our study has limitations. Due to premature discontinuation, a small number of patients was enrolled. However, patients monitoring was careful with reliable AT samples withdrawn before and 6 months after the switch, allowing individual comparison. We could not verify the individual level of gene expression nor the change in protein expression and therefore our propositions regarding gene expression variations remain hypothetical. We cannot address the effect of raltegravir *versus* maraviroc. As well, we cannot analyze the effect of each ART molecules received before switching. Insulin resistance was evaluated by using the surrogate QUICKI index based only on fasting glucose and insulin levels but which was shown more accurate than HOMA-IR[15].

In conclusion, in a small group of well-controlled PLWH, we observed that raltegravir/maraviroc markedly altered AT transcriptome suggesting increased adipogenesis, probably latter resulting in fat mass gain. Also, insulin resistance increased stressing for the risk of diabetes, requiring a careful follow-up. However, we observed a striking reduction in the expression of immune/inflammation-related genes. These

preliminary lead to interesting hypotheses which need to be confirmed in larger studies as they may impact the use of INSTI in some populations.

**Legend of figures**

**Figure 1**: Network analysis with the GO biological process annotation of genes with altered expression 6 months after switch to raltegravir/maraviroc

Green: decreased expression

Red: increased expression

**Supplemental Figure 1**: Significance Analysis of Microarrays (SAM) analysis of comparative adipose tissue gene expression after versus before the switch to raltegravir/maraviroc

**Supplemental Figure 2**: Functional analysis by using the KEGG database of adipose tissue genes up- or down-regulated after switch to raltegravir/maraviroc

Green: decreased expression

Red: increased expression

**Acknowledgements**

We thank the clinical research department from ANRS for their support regarding the management of the ROCnRAL study. We thank Ginette Marlin for evaluation of the adipokines and inflammatory markers.

JPB performed all the lipoaspirations.

VP, RA, JPB, SF, EC and EP have performed all the assays presented in this paper and participated to their analysis.

LA has monitored the ROCnRAL study

VP, LA, JPB and JC have performed the analysis of the data

CK has participated to the study as the PI of the ROCnRAL study

JPB, JC, CK and KC have written the grant proposition

JC has written the first draft, BF, JAW, KC and CK have participated to the redaction and all the authors have participated to the correction of the paper

**References**

1. Koethe JR, Lagathu C, Lake JE, Domingo P, Calmy A, Falutz J, et al. **HIV and antiretroviral therapy-related fat alterations**. *Nat Rev Dis Primers* 2020; 6(1):48.

2. Gorwood J, Bourgeois C, Pourcher V, Pourcher G, Charlotte F, Mantecon M, et al. **The integrase inhibitors dolutegravir and raltegravir exert pro-adipogenic and profibrotic effects and induce insulin resistance in human/simian adipose tissue and human adipocytes**. *Clin Infect Dis* 2020.

3. Katlama C, Assoumou L, Valantin MA, Soulie C, Duvivier C, Chablais L, et al. **Maraviroc plus raltegravir failed to maintain virological suppression in HIV-infected patients with lipohypertrophy: results from the ROCnRAL ANRS 157 study**. *J Antimicrob Chemother* 2014; 69(6):1648-1652.

4. Martinez E, D'Albuquerque PM, Llibre JM, Gutierrez F, Podzamczer D, Antela A, et al. **Changes in cardiovascular biomarkers in HIV-infected patients switching from ritonavir-boosted protease inhibitors to raltegravir**. *AIDS* 2012; 26(18):2315-2326.

5. Katlama C, Assoumou L, Valantin MA, Soulie C, Martinez E, Beniguel L, et al. **Dual therapy combining raltegravir with etravirine maintains a high level of viral suppression over 96 weeks in long-term experienced HIV-infected individuals over 45 years on a PI-based regimen: results from the Phase II ANRS 163 ETRAL study**. *J Antimicrob Chemother* 2019; 74(9):2742-2751.

6. Gatell JM, Assoumou L, Moyle G, Waters L, Johnson M, Domingo P, et al. **Immediate Versus Deferred Switching From a Boosted Protease Inhibitor-based Regimen to a Dolutegravir-based Regimen in Virologically Suppressed Patients With High**

**Cardiovascular Risk or Age >/=50 Years: Final 96-Week Results of the NEAT022 Study**. *Clin Infect Dis* 2019; 68(4):597-606.

7. Assoumou L, di Clemente N, Fellahi S, Beniguel L, Bastard JP, Feve B, et al. **Impact of the reproductive/hormonal status on weight, fat and insulin resistance in HIV-infected women switching from a PI regimen to dual raltegravir-etravirine therapy: results from the ANRS163-ETRAL trial at 48 and 96 weeks**. *HIV Med* 2019; 20(SI 9):132.

8. Francisci D, Pirro M, Schiaroli E, Mannarino MR, Cipriani S, Bianconi V, et al. **Maraviroc Intensification Modulates Atherosclerotic Progression in HIV-Suppressed Patients at High Cardiovascular Risk. A Randomized, Crossover Pilot Study**. *Open Forum Infect Dis* 2019; 6(4):ofz112.

9. Piconi S, Pocaterra D, Rainone V, Cossu M, Masetti M, Rizzardini G, et al. **Maraviroc Reduces Arterial Stiffness in PI-Treated HIV-infected Patients**. *Sci Rep* 2016; 6:28853.

10. Gonzalez EO, Boix V, Deltoro MG, Aldeguer JL, Portilla J, Montero M, et al. **The effects of Maraviroc on liver fibrosis in HIV/HCV co-infected patients**. *J Int AIDS Soc* 2014; 17(4 Suppl 3):19643.

11. Bradshaw D, Gilleece Y, Verma S, Abramowicz I, Bremner S, Perry N. **Protocol for a phase IV, open-label feasibility study investigating non-invasive markers of hepatic fibrosis in people living with HIV-1 and non-alcoholic fatty liver disease randomised to receiving optimised background therapy (OBT) plus maraviroc or OBT alone**. *BMJ Open* 2020; 10(7):e035596.

12. Bastard JP, Fellahi S, Couffignal C, Raffi F, Gras G, Hardel L, et al. **Increased systemic immune activation and inflammatory profile of long-term HIV-infected ART-controlled**

**patients is related to personal factors, but not to markers of HIV infection severity**. *J Antimicrob Chemother* 2015; 70(6):1816-1824.

13. Gorwood J, Bourgeois C, Mantecon M, Atlan M, Pourcher V, Pourcher G, et al. **Impact of HIV/simian immunodeficiency virus infection and viral proteins on adipose tissue fibrosis and adipogenesis**. *AIDS* 2019; 33(6):953-964.

14. Lacroix D, Moutel S, Coupaye M, Huvenne H, Faucher P, Pelloux V, et al. **Metabolic and adipose tissue signatures in adults with Prader-Willi syndrome: a model of extreme adiposity**. *J Clin Endocrinol Metab* 2015; 100(3):850-859.

15. Rabasa-Lhoret R, Bastard JP, Jan V, Ducluzeau P, Andreelli F, Guerbre F, et al. **Modified quantitative insulin sensitivity check index is better correlated to hyperinsulinemic glucose clamp than other fasting-based index of insulin sesnitivity in different insulin-resistant states**. *J Clin Endocrinol Metab* 2003; 88(10):4917-4923.

16. Diaz-Delfin J, Domingo P, Giralt M, Villarroya F. **Maraviroc reduces cytokine expression and secretion in human adipose cells without altering adipogenic differentiation**. *Cytokine* 2013; 61(3):808-815.

17. Pourcher V, Dutoit Y, Capeau J, Boccara F, Soulie C, Ndoadoumgue A, et al. **Characteristics of HIV+ and HIV- patients undergoing bariatric surgery: ObeVIH study**. In: *virtual CROI scientific spotlight-TM ID1717*. virtual; 2021.

18. Guaraldi G, Draisci J, Milic J, Carli F, Besutti G, Bassoli C, et al. **Fat distribution and ensity in people living with HIV with ≥5% weight gain**. *J Intern AIDS Soc* 2020; 23(S7):E25616.

19. Perez-Matute P, Pichel JG, Iniguez M, Recio-Fernandez E, Perez-Martinez L, Torrens R, et al. **Maraviroc ameliorates the increased adipose tissue macrophage recruitment**

**induced by a high-fat diet in a mouse model of obesity**. *Antivir Ther* 2017; 22(2):163-168.

20. Auclair M, Guenantin AC, Fellahi S, Garcia M, Capeau J. **HIV antiretroviral drugs, dolutegravir, maraviroc and ritonavir-boosted atazanavir use different pathways to affect inflammation, senescence and insulin sensitivity in human coronary endothelial cells**. *PLoS One* 2020; 15(1):e0226924.

21. Assoumou L, Racine C, Fellahi S, Lamaziere A, Farabos D, Beniguel L, et al. **Fat gain differs by sex and hormonal status in persons living with suppressed HIV switched to raltegravir/etravirine**. *AIDS* 2020; 34(12):1859-1862.

22. Divoux A, Tordjman J, Lacasa D, Veyrie N, Hugol D, Aissat A, et al. **Fibrosis in human adipose tissue: composition, distribution, and link with lipid metabolism and fat mass loss**. *Diabetes* 2010; 59(11):2817-2825.

23. Martinez E, Assoumou L, Moyle G, Waters L, Johnson M, Domingo P, et al. **48-week changes in biomarkers in subjects with high cardiovascular risk boosted switching from ritonavir-protease inhibitors to dolutegravir: the NEAT022 study**. *Journal of the International AIDS Society* 2018; 21(S8):e25187.

**Table 1**

**Characteristics of PLWH included in the ROCnRAL sub-study with paired adipose tissue biopsies: clinical and metabolic parameters, adipokines and inflammatory markers, adipose tissue parameters.**

The results are expressed as mean (SEM). The differences between T0 (inclusion) and T*end* was calculated by using the Wilcoxon-paired test.

| | T0 | T*end* | *P* |
|---|---|---|---|
| CD4 cells/mm$^3$ | 699 (56) | 612 (23) | 0.219 |
| CD8 cells/mm$^3$ | 786 (100) | 820 (111) | 0.359 |
| BMI kg/m$^2$ | 26.1 (1.2) | 26.4 (1.3) | 0.578 |
| WC cm | 94.6 (2.2) | 97.9 (4.0) | 0.250 |
| HC cm | 94.9 (1.8) | 99.1 (2.1) | **0.031** |
| WHR | 1.00 (0.02) | 0.98 (0.02) | 0.250 |
| Trunk fat kg | 13.2 (1.4) | 13.6 (1.8) | 0.562 |
| Limb fat kg | 8.0 (1.2) | 8.1 (1.2) | 0.312 |
| Glycemia mmol/L | 5.1 (0.2) | 5.5 (0.25) | 0.250 |
| Triglycerides mmol/L | 2.0 (0.9) | 1.3 (0.2) | 0.437 |
| HDL-cholesterol mmol/L | 1.35 (0.14) | 1.5 (0.12) | 0.219 |
| LDL-cholesterol mmol/L | 3.3 (0.33) | 2.8 (0.24) | 0.219 |
| Insulinemia mU/L | 10.7 (1.8) | 21.5 (10.0) | **0.047** |
| QUICKI | 0.342 (0.011) | 0.315 (0.017) | **0.046** |

| | | | |
|---|---|---|---|
| hsCRP mg/L | 2.61 (1.06) | 3.8 (1.7) | 0.578 |
| hsIL-6 pg/L | 4.5 (2.5) | 2.7 (0.9) | 0.937 |
| Adiponectin mg/L | 3.9 (0.8) | 4.4 (1.1) | 0.937 |
| Leptin μg/L | 12.4 (4.4) | 18.2 (5.1) | 0.078 |
| sCD14 ng/ml | 1583 (71) | 1471 (101) | 0.219 |
| sCD163 ng/ml | 699 (103) | 790 (151) | 0.467 |
| Adipocyte diameter μm | 106.9 (2.1) | 113 (4.1) | 0.109 |
| Adipocyte volume $x10^3 \mu m^3$ | 649 (38) | 776 (78) | 0.109 |
| Adipose tissue fibrosis AU | 1.37 (0.26) | 1.56 (0.35) | 0.999 |

WC: waist circumference, HC: hip circumference, WHR: waist to hip ratio, HDL: high density lipoproteins, LDL: low density lipoproteins, AU: arbitrary unit

**Figure 1**

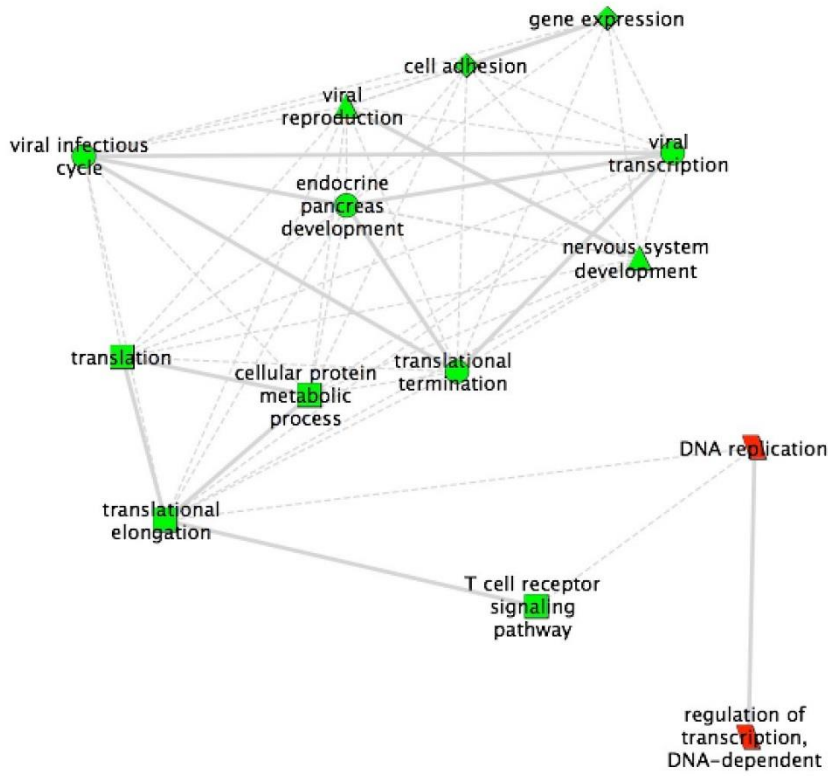


Green: decreased expression
Red: increased expression

| Gene ID | ID | Gene symbol | Name | Fold Change | p-value(% |
|---|---|---|---|---|---|
| ILMN_16829 | 4818 | NKG7 | natural killer cell group 7 sequence | 0,7 | 1,8141 |
| ILMN_23776 | 919 | CD247 | CD247 molecule | 0,7 | 1,2499 |
| ILMN_21206 | 7102 | TSPAN7 | tetraspanin 7 | 0,7 | 1,8141 |
| ILMN_16768 | 84417 | C2orf40 | chromosome 2 open reading frame 40 | 0,7 | 2,0799 |
| ILMN_21094 | 3002 | GZMB | granzyme B (granzyme 2, cytotoxic T-ly | 0,7 | 2,0799 |
| ILMN_17695 | 83700 | JAM3 | junctional adhesion molecule 3 | 0,7 | 1,5007 |
| ILMN_17494 | 8502 | PKP4 | plakophilin 4 | 0,7 | 2,0799 |
| ILMN_21122 | 7293 | TNFRSF4 | tumor necrosis factor receptor superfa | 0,7 | 2,6244 |
| ILMN_22090 | 6231 | RPS26 | ribosomal protein S26 | 0,7 | 2,0799 |
| ILMN_16769 | 919 | CD247 | CD247 molecule | 0,7 | 1,5007 |
| ILMN_20862 | 114826 | SMYD4 | SET and MYND domain containing 4 | 0,7 | 2,0799 |
| ILMN_17875 | 8848 | TSC22D1 | TSC22 domain family, member 1 | 0,7 | 1,2499 |
| ILMN_32368 | 57523 | NYNRIN | NYN domain and retroviral integrase cc | 0,7 | 2,0799 |
| ILMN_24063 | 10616 | RBCK1 | RanBP-type and C3HC4-type zinc finger | 0,7 | 2,0799 |
| ILMN_17707 | 83543 | AIF1L | allograft inflammatory factor 1-like | 0,7 | 2,0799 |
| ILMN_32517 | 79002 | C19orf43 | chromosome 19 open reading frame 43 | 0,7 | 2,6244 |
| ILMN_22614 | 915 | CD3D | CD3d molecule, delta (CD3-TCR comple | 0,7 | 1,2499 |
| ILMN_21123 | 10589 | DRAP1 | DR1-associated protein 1 (negative cofa | 0,7 | 2,6244 |
| ILMN_16723 | 58494 | JAM2 | junctional adhesion molecule 2 | 0,7 | 0,0000 |
| ILMN_17696 | 5878 | RAB5C | RAB5C, member RAS oncogene family | 0,7 | 2,6244 |
| ILMN_16913 | 3575 | IL7R | interleukin 7 receptor | 0,7 | 1,8141 |
| ILMN_23162 | 84525 | HOPX | HOP homeobox | 0,7 | 1,5007 |
| ILMN_17484 | 55303 | GIMAP4 | GTPase, IMAP family member 4 | 0,7 | 2,0799 |
| ILMN_17171 | 3476 | IGBP1 | immunoglobulin (CD79A) binding prote | 0,8 | 2,0799 |
| ILMN_32502 | 29767 | TMOD2 | tropomodulin 2 (neuronal) | 0,8 | 1,8141 |
| ILMN_17816 | 716 | C1S | complement component 1, s subcompc | 0,8 | 1,8141 |
| ILMN_17761 | 283298 | OLFML1 | olfactomedin-like 1 | 0,8 | 0,8244 |
| ILMN_31889 | 441951 | C20orf199 | ZNFX1 antisense RNA 1 (non-protein co | 0,8 | 1,0331 |
| ILMN_32433 | 343990 | C2orf55 | chromosome 2 open reading frame 55 | 0,8 | 0,0000 |
| ILMN_17319 | 6329 | SCN4A | sodium channel, voltage-gated, type IV | 0,8 | 1,8141 |
| ILMN_16704 | 79171 | RBM42 | RNA binding motif protein 42 | 0,8 | 2,6244 |
| ILMN_21748 | 146894 | CD300LG | CD300 molecule-like family member g | 0,8 | 2,0799 |
| ILMN_17852 | 965 | CD58 | CD58 molecule | 0,8 | 2,0799 |
| ILMN_18057 | 5214 | PFKP | phosphofructokinase, platelet | 0,8 | 2,6244 |
| ILMN_16875 | 10507 | SEMA4D | sema domain, immunoglobulin domain | 0,8 | 1,2499 |
| ILMN_16512 | 255877 | BCL6B | B-cell CLL/lymphoma 6, member B | 0,8 | 2,6244 |
| ILMN_16984 | 3609 | ILF3 | interleukin enhancer binding factor 3, 9 | 0,8 | 2,0799 |
| ILMN_23882 | 9862 | MED24 | mediator complex subunit 24 | 0,8 | 2,6244 |
| ILMN_18060 | 5720 | PSME1 | proteasome (prosome, macropain) acti | 0,8 | 2,6244 |
| ILMN_23841 | 9289 | GPR56 | G protein-coupled receptor 56 | 0,8 | 1,8141 |
| ILMN_17695 | 54453 | RIN2 | Ras and Rab interactor 2 | 0,8 | 2,0799 |
| ILMN_17545 | 9828 | ARHGEF17 | Rho guanine nucleotide exchange facto | 0,8 | 1,5007 |
| ILMN_16890 | 79673 | ZNF329 | zinc finger protein 329 | 0,8 | 2,6244 |
| ILMN_16582 | 6139 | RPL17 | ribosomal protein L17 | 0,8 | 1,8141 |
| ILMN_32514 | 9804 | TOMM20 | translocase of outer mitochondrial mer | 0,8 | 1,5007 |

| | | | | | |
|---|---|---|---|---|---|
| ILMN_21574 | 3122 | HLA-DRA | major histocompatibility complex, class | 0,8 | 2,6244 |
| ILMN_17478 | 6605 | SMARCE1 | SWI/SNF related, matrix associated, act | 0,8 | 2,0799 |
| ILMN_17959 | 116988 | CENTG3 | ArfGAP with GTPase domain, ankyrin re | 0,8 | 2,6244 |
| ILMN_23258 | 915 | CD3D | CD3d molecule, delta (CD3-TCR comple | 0,8 | 2,6244 |
| ILMN_16857 | 1974 | EIF4A2 | eukaryotic translation initiation factor 4 | 0,8 | 1,5007 |
| ILMN_18044 | 57228 | SMAGP | small cell adhesion glycoprotein | 0,8 | 1,5007 |
| ILMN_18134 | 5092 | PCBD1 | pterin-4 alpha-carbinolamine dehydrat | 0,8 | 2,6244 |
| ILMN_16535 | 1901 | EDG1 | sphingosine-1-phosphate receptor 1 | 0,8 | 2,6244 |
| ILMN_17217 | 54707 | ATPBD1B | GPN-loop GTPase 2 | 0,8 | 2,6244 |
| ILMN_32438 | 4695 | NDUFA2 | NADH dehydrogenase (ubiquinone) 1 a | 0,8 | 1,0331 |
| ILMN_16608 | 6050 | RNH1 | ribonuclease/angiogenin inhibitor 1 | 0,8 | 2,6244 |
| ILMN_17303 | 84317 | CCDC115 | coiled-coil domain containing 115 | 0,8 | 2,0799 |
| ILMN_16597 | 689 | BTF3 | basic transcription factor 3 | 0,8 | 1,5007 |
| ILMN_22537 | 7903 | ST8SIA4 | ST8 alpha-N-acetyl-neuraminide alpha- | 0,8 | 1,8141 |
| ILMN_21202 | 10231 | RCAN2 | regulator of calcineurin 2 | 0,8 | 2,6244 |
| ILMN_17433 | 113189 | CHST14 | carbohydrate (N-acetylgalactosamine 4 | 0,8 | 2,6244 |
| ILMN_17592 | 118 | ADD1 | adducin 1 (alpha) | 0,8 | 1,2499 |
| ILMN_16768 | 116835 | HSPA12B | heat shock 70kD protein 12B | 0,8 | 1,8141 |
| ILMN_17690 | 5547 | PRCP | prolylcarboxypeptidase (angiotensinase | 0,8 | 2,0799 |
| ILMN_23402 | 5142 | PDE4B | phosphodiesterase 4B, cAMP-specific | 0,8 | 0,0000 |
| ILMN_18007 | 23180 | RFTN1 | raftlin, lipid raft linker 1 | 0,8 | 2,6244 |
| ILMN_23372 | 6210 | RPS15A | ribosomal protein S15a | 0,8 | 1,0331 |
| ILMN_16780 | 9425 | CDYL | chromodomain protein, Y-like | 0,8 | 1,8141 |
| ILMN_16590 | 3111 | HLA-DOA | major histocompatibility complex, class | 0,8 | 1,8141 |
| ILMN_18083 | 9744 | ACAP1 | ArfGAP with coiled-coil, ankyrin repeat | 0,8 | 2,0799 |
| ILMN_16804 | 6748 | SSR4 | signal sequence receptor, delta | 0,8 | 2,6244 |
| ILMN_20796 | 3820 | KLRB1 | killer cell lectin-like receptor subfamily | 0,8 | 1,2499 |
| ILMN_18129 | 116159 | CYYR1 | cysteine/tyrosine-rich 1 | 0,8 | 2,0799 |
| ILMN_17973 | 23048 | FNBP1 | formin binding protein 1 | 0,8 | 2,0799 |
| ILMN_17823 | 5430 | POLR2A | polymerase (RNA) II (DNA directed) pol | 0,8 | 1,5007 |
| ILMN_22050 | 57692 | MAGEE1 | melanoma antigen family E, 1 | 0,8 | 2,0799 |
| ILMN_23520 | 9289 | GPR56 | G protein-coupled receptor 56 | 0,8 | 0,0000 |
| ILMN_17917 | 1375 | CPT1B | carnitine palmitoyltransferase 1B (musc | 0,8 | 2,6244 |
| ILMN_16797 | 104 | ADARB1 | adenosine deaminase, RNA-specific, B1 | 0,8 | 2,6244 |
| ILMN_23830 | 6139 | RPL17 | ribosomal protein L17 | 0,8 | 2,0799 |
| ILMN_23251 | 408 | ARRB1 | arrestin, beta 1 | 0,8 | 0,8244 |
| ILMN_18038 | 84518 | CNFN | cornifelin | 0,8 | 2,6244 |
| ILMN_16680 | 90952 | ESAM | endothelial cell adhesion molecule | 0,8 | 2,6244 |
| ILMN_17775 | 3695 | ITGB7 | integrin, beta 7 | 0,8 | 1,5007 |
| ILMN_16657 | 1434 | CSE1L | CSE1 chromosome segregation 1-like (y | 0,8 | 2,6244 |
| ILMN_23523 | 9770 | RASSF2 | Ras association (RalGDS/AF-6) domain f | 0,8 | 2,6244 |
| ILMN_18151 | 4628 | MYH10 | myosin, heavy chain 10, non-muscle | 0,8 | 2,6244 |
| ILMN_16772 | 55217 | TMLHE | trimethyllysine hydroxylase, epsilon | 0,8 | 2,0799 |
| ILMN_16519 | 8460 | TPST1 | tyrosylprotein sulfotransferase 1 | 0,8 | 1,2499 |
| ILMN_16779 | 51292 | GMPR2 | guanosine monophosphate reductase 2 | 0,8 | 1,2499 |
| ILMN_21179 | 7570 | ZNF22 | zinc finger protein 22 (KOX 15) | 0,8 | 2,6244 |

| | | | | | |
|---|---|---|---|---|---|
| ILMN_17006( | 84282 | RNF135 | ring finger protein 135 | 0,8 | 2,6244 |
| ILMN_17808( | 5583 | PRKCH | protein kinase C, eta | 0,8 | 0,7857 |
| ILMN_17754( | 5217 | PFN2 | profilin 2 | 0,8 | 2,6244 |
| ILMN_17754( | 8082 | SSPN | sarcospan | 0,8 | 2,0799 |
| ILMN_32394( | 100128927 | ZBTB42 | zinc finger and BTB domain containing ( | 0,8 | 1,5007 |
| ILMN_17975( | 84269 | CHCHD5 | coiled-coil-helix-coiled-coil-helix domai | 0,8 | 2,6244 |
| ILMN_21916( | 51142 | CHCHD2 | coiled-coil-helix-coiled-coil-helix domai | 0,8 | 2,0799 |
| ILMN_16940( | 27335 | EIF3K | eukaryotic translation initiation factor 3 | 0,8 | 0,8244 |
| ILMN_17813( | 5239 | PGM5 | phosphoglucomutase 5 | 0,8 | 1,8141 |
| ILMN_17513( | 10616 | RBCK1 | RanBP-type and C3HC4-type zinc finger | 0,8 | 1,8141 |
| ILMN_16557( | 54460 | MRPS21 | mitochondrial ribosomal protein S21 | 0,8 | 1,8141 |
| ILMN_17831( | 6192 | RPS4Y1 | ribosomal protein S4, Y-linked 1 | 0,8 | 1,5007 |
| ILMN_23265( | 834 | CASP1 | caspase 1, apoptosis-related cysteine p | 0,8 | 2,6244 |
| ILMN_20870( | 54543 | TOMM7 | translocase of outer mitochondrial mer | 0,8 | 2,0799 |
| ILMN_17395( | 78987 | CRELD1 | cysteine-rich with EGF-like domains 1 | 0,8 | 1,2499 |
| ILMN_17095( | 5239 | PGM5 | phosphoglucomutase 5 | 0,8 | 1,8141 |
| ILMN_18113( | 2494 | NR5A2 | nuclear receptor subfamily 5, group A, | 0,8 | 1,8141 |
| ILMN_17761( | 5414 | 38231 | septin 4 | 0,8 | 1,8141 |
| ILMN_17357( | 3764 | KCNJ8 | potassium inwardly-rectifying channel, | 0,8 | 2,0799 |
| ILMN_17558( | 85360 | SYDE1 | synapse defective 1, Rho GTPase, homo | 0,8 | 2,0799 |
| ILMN_20876( | 79901 | CYBRD1 | cytochrome b reductase 1 | 0,8 | 2,0799 |
| ILMN_23826( | 11043 | MID2 | midline 2 | 0,8 | 2,0799 |
| ILMN_21676( | 4666 | NACA | nascent polypeptide-associated comple | 0,8 | 2,0799 |
| ILMN_21545( | 4736 | RPL10A | ribosomal protein L10a | 0,8 | 2,0799 |
| ILMN_16711( | 2701 | GJA4 | gap junction protein, alpha 4, 37kDa | 0,8 | 1,0331 |
| ILMN_23345( | 3183 | HNRNPC | heterogeneous nuclear ribonucleoprot | 0,8 | 2,0799 |
| ILMN_16568( | 5947 | RBP1 | retinol binding protein 1, cellular | 0,8 | 2,6244 |
| ILMN_16990( | 8550 | MAPKAPK5 | mitogen-activated protein kinase-activa | 0,8 | 1,0331 |
| ILMN_21399( | 6189 | RPS3A | ribosomal protein S3A | 0,8 | 0,8244 |
| ILMN_17365( | 151473 | SLC16A14 | solute carrier family 16, member 14 (m | 0,8 | 1,5007 |
| ILMN_17116( | 25824 | PRDX5 | peroxiredoxin 5 | 0,8 | 1,5007 |
| ILMN_22269( | 9766 | KIAA0247 | KIAA0247 | 0,8 | 2,0799 |
| ILMN_23685( | 115290 | FBXO17 | F-box protein 17 | 0,8 | 2,0799 |
| ILMN_17115( | 1690 | COCH | coagulation factor C homolog, cochlin ( | 0,8 | 1,2499 |
| ILMN_17612( | 2132 | EXT2 | exostosin 2 | 0,8 | 1,5007 |
| ILMN_20730( | 94107 | TMEM203 | transmembrane protein 203 | 0,8 | 2,0799 |
| ILMN_17496( | 8454 | CUL1 | cullin 1 | 0,8 | 1,0331 |
| ILMN_17164( | 65057 | ACD | adrenocortical dysplasia homolog (mou | 0,8 | 1,2499 |
| ILMN_16740( | 54543 | TOMM7 | translocase of outer mitochondrial mer | 0,8 | 1,2499 |
| ILMN_23194( | 689 | BTF3 | basic transcription factor 3 | 0,8 | 2,0799 |
| ILMN_17627( | 6138 | RPL15 | ribosomal protein L15 | 0,8 | 1,5007 |
| ILMN_17651( | 3455 | IFNAR2 | interferon (alpha, beta and omega) rec | 0,8 | 2,6244 |
| ILMN_17394( | 5396 | PRRX1 | paired related homeobox 1 | 0,8 | 2,6244 |
| ILMN_16920( | 4692 | NDN | necdin homolog (mouse) | 0,8 | 2,6244 |
| ILMN_17494( | 64983 | MRPL32 | mitochondrial ribosomal protein L32 | 0,8 | 1,8141 |
| ILMN_18104( | 83871 | RAB34 | RAB34, member RAS oncogene family | 0,8 | 1,2499 |

| | | | | | |
|---|---|---|---|---|---|
| ILMN_17306 | 408 | ARRB1 | arrestin, beta 1 | 0,8 | 2,0799 |
| ILMN_18102 | 90423 | ATP6V1E2 | ATPase, H+ transporting, lysosomal 31k | 0,8 | 2,0799 |
| ILMN_21012 | 64407 | RGS18 | regulator of G-protein signaling 18 | 0,8 | 1,5007 |
| ILMN_32453 | 84747 | UNC119B | unc-119 homolog B (C. elegans) | 0,8 | 2,6244 |
| ILMN_18116 | 117246 | FTSJ3 | FtsJ homolog 3 (E. coli) | 0,8 | 2,6244 |
| ILMN_16801 | 55353 | LAPTM4B | lysosomal protein transmembrane 4 be | 0,8 | 2,0799 |
| ILMN_17611 | 286257 | C9orf142 | chromosome 9 open reading frame 142 | 0,8 | 1,2499 |
| ILMN_17145 | 79026 | AHNAK | AHNAK nucleoprotein | 0,8 | 0,0000 |
| ILMN_16787 | 6993 | DYNLT1 | dynein, light chain, Tctex-type 1 | 0,8 | 2,0799 |
| ILMN_24002 | 6717 | SRI | sorcin | 0,8 | 2,6244 |
| ILMN_17601 | 11043 | MID2 | midline 2 | 0,8 | 1,8141 |
| ILMN_17204 | 5253 | PHF2 | PHD finger protein 2 | 0,8 | 1,8141 |
| ILMN_18031 | 23450 | SF3B3 | splicing factor 3b, subunit 3, 130kDa | 0,8 | 1,2499 |
| ILMN_18026 | 83468 | GLT8D2 | glycosyltransferase 8 domain containin | 0,8 | 1,8141 |
| ILMN_20873 | 55113 | XKR8 | XK, Kell blood group complex subunit-r | 0,8 | 1,5007 |
| ILMN_32388 | 23248 | RPRD2 | regulation of nuclear pre-mRNA domai | 0,8 | 0,0000 |
| ILMN_18089 | 6194 | RPS6 | ribosomal protein S6 | 0,8 | 1,2499 |
| ILMN_17383 | 1938 | EEF2 | eukaryotic translation elongation factor | 0,8 | 2,0799 |
| ILMN_18007 | 6167 | RPL37 | ribosomal protein L37 | 0,8 | 2,6244 |
| ILMN_23159 | 81606 | LBH | limb bud and heart development homo | 0,8 | 2,0799 |
| ILMN_16523 | 222223 | KIAA1324L | KIAA1324-like | 0,8 | 2,6244 |
| ILMN_17247 | 8440 | NCK2 | NCK adaptor protein 2 | 0,9 | 1,5007 |
| ILMN_16593 | 26610 | ELP4 | elongation protein 4 homolog (S. cerev | 0,9 | 2,6244 |
| ILMN_17375 | 6874 | TAF4 | TAF4 RNA polymerase II, TATA box binc | 0,9 | 1,8141 |
| ILMN_17845 | 6383 | SDC2 | syndecan 2 | 0,9 | 2,6244 |
| ILMN_17202 | 64806 | IL25 | interleukin 25 | 0,9 | 0,8244 |
| ILMN_17189 | 9802 | DAZAP2 | DAZ associated protein 2 | 0,9 | 0,0000 |
| ILMN_17490 | 3115 | HLA-DPB1 | major histocompatibility complex, class | 0,9 | 2,0799 |
| ILMN_17629 | 9812 | KIAA0141 | KIAA0141 | 0,9 | 1,2499 |
| ILMN_17719 | 57153 | SLC44A2 | solute carrier family 44, member 2 | 0,9 | 1,8141 |
| ILMN_17671 | 54816 | ZNF280D | zinc finger protein 280D | 0,9 | 1,8141 |
| ILMN_17421 | 83743 | GRWD1 | glutamate-rich WD repeat containing 1 | 0,9 | 1,0331 |
| ILMN_16525 | 89853 | FAM125B | family with sequence similarity 125, me | 0,9 | 1,2499 |
| ILMN_17287 | 221395 | GPR116 | G protein-coupled receptor 116 | 0,9 | 2,6244 |
| ILMN_17734 | 6764 | ST5 | suppression of tumorigenicity 5 | 0,9 | 2,0799 |
| ILMN_16900 | 9270 | ITGB1BP1 | integrin beta 1 binding protein 1 | 0,9 | 2,6244 |
| ILMN_17737 | 65005 | MRPL9 | mitochondrial ribosomal protein L9 | 0,9 | 2,6244 |
| ILMN_21018 | 55353 | LAPTM4B | lysosomal protein transmembrane 4 be | 0,9 | 1,8141 |
| ILMN_17313 | 55486 | PARL | presenilin associated, rhomboid-like | 0,9 | 1,5007 |
| ILMN_32395 | 401115 | C4orf48 | chromosome 4 open reading frame 48 | 0,9 | 2,6244 |
| ILMN_17022 | 79630 | C1orf54 | chromosome 1 open reading frame 54 | 0,9 | 2,6244 |
| ILMN_17791 | 23384 | CYTSA | sperm antigen with calponin homology | 0,9 | 2,0799 |
| ILMN_17291 | 55069 | C7orf42 | transmembrane protein 248 | 0,9 | 2,6244 |
| ILMN_16827 | 8463 | TEAD2 | TEA domain family member 2 | 0,9 | 1,0331 |
| ILMN_17975 | 116841 | SNAP47 | synaptosomal-associated protein, 47kD | 0,9 | 2,0799 |
| ILMN_16893 | 83443 | SF3B5 | splicing factor 3b, subunit 5, 10kDa | 0,9 | 2,0799 |

| | | | | | |
|---|---|---|---|---|---|
| ILMN_17397 | 126792 | B3GALT6 | UDP-Gal:betaGal beta 1,3-galactosyltra | 0,9 | 2,6244 |
| ILMN_17063 | 51241 | C14orf112 | COX16 cytochrome c oxidase assembly | 0,9 | 2,6244 |
| ILMN_17618 | 90411 | MCFD2 | multiple coagulation factor deficiency 2 | 0,9 | 2,0799 |
| ILMN_17172 | 10544 | PROCR | protein C receptor, endothelial | 0,9 | 2,0799 |
| ILMN_16830 | 5504 | PPP1R2 | protein phosphatase 1, regulatory (inhi | 0,9 | 2,6244 |
| ILMN_16663 | 93058 | COQ10A | coenzyme Q10 homolog A (S. cerevisiae | 0,9 | 2,6244 |
| ILMN_16796 | 27352 | SGSM3 | small G protein signaling modulator 3 | 0,9 | 1,8141 |
| ILMN_17256 | 6612 | SUMO3 | SMT3 suppressor of mif two 3 homolog | 0,9 | 1,5007 |
| ILMN_23521 | 2064 | ERBB2 | v-erb-b2 erythroblastic leukemia viral o | 0,9 | 1,5007 |
| ILMN_16743 | 10971 | YWHAQ | tyrosine 3-monooxygenase/tryptophan | 0,9 | 1,5007 |
| ILMN_21988 | 2230 | FDX1 | ferredoxin 1 | 0,9 | 2,0799 |
| ILMN_16911 | 116092 | DNTTIP1 | deoxynucleotidyltransferase, terminal, | 0,9 | 0,8244 |
| ILMN_24081 | 24144 | TFIP11 | tuftelin interacting protein 11 | 0,9 | 2,0799 |
| ILMN_16765 | 5654 | HTRA1 | HtrA serine peptidase 1 | 0,9 | 0,8244 |
| ILMN_16767 | 4236 | MFAP1 | microfibrillar-associated protein 1 | 0,9 | 2,0799 |
| ILMN_16949 | 5780 | PTPN9 | protein tyrosine phosphatase, non-rece | 0,9 | 2,6244 |
| ILMN_18019 | 10465 | PPIH | peptidylprolyl isomerase H (cyclophilin | 0,9 | 0,8244 |
| ILMN_16784 | 1123 | CHN1 | chimerin (chimaerin) 1 | 0,9 | 2,6244 |
| ILMN_18129 | 10695 | CNPY3 | canopy 3 homolog (zebrafish) | 0,9 | 2,0799 |
| ILMN_17970 | 10436 | EMG1 | EMG1 nucleolar protein homolog (S. ce | 0,9 | 2,0799 |
| ILMN_22343 | 80772 | GLTPD1 | glycolipid transfer protein domain cont | 0,9 | 1,0331 |
| ILMN_20555 | 55790 | CSGALNACT1 | chondroitin sulfate N-acetylgalactosam | 0,9 | 1,2499 |
| ILMN_16702 | 26020 | LRP10 | low density lipoprotein receptor-relate | 0,9 | 0,8244 |
| ILMN_16971 | 51759 | C9orf78 | chromosome 9 open reading frame 78 | 0,9 | 1,5007 |
| ILMN_17032 | 112970 | KTI12 | KTI12 homolog, chromatin associated ( | 0,9 | 2,6244 |
| ILMN_16772 | 11178 | LZTS1 | leucine zipper, putative tumor suppress | 0,9 | 1,8141 |
| ILMN_16934 | 23478 | SEC11A | SEC11 homolog A (S. cerevisiae) | 0,9 | 2,6244 |
| ILMN_18075 | 55181 | C17orf71 | smg-8 homolog, nonsense mediated m | 0,9 | 1,8141 |
| ILMN_17351 | 57019 | CIAPIN1 | cytokine induced apoptosis inhibitor 1 | 0,9 | 1,8141 |
| ILMN_17200 | 30844 | EHD4 | EH-domain containing 4 | 0,9 | 1,2499 |
| ILMN_17021 | 2739 | GLO1 | glyoxalase I | 0,9 | 2,6244 |
| ILMN_16724 | 6135 | RPL11 | ribosomal protein L11 | 0,9 | 2,6244 |
| ILMN_16878 | 22928 | SEPHS2 | selenophosphate synthetase 2 | 0,9 | 2,6244 |
| ILMN_16515 | 8603 | FAM193A | family with sequence similarity 193, me | 0,9 | 2,0799 |
| ILMN_16692 | 7564 | ZNF16 | zinc finger protein 16 | 0,9 | 1,8141 |
| ILMN_17433 | 7265 | TTC1 | tetratricopeptide repeat domain 1 | 0,9 | 1,0331 |
| ILMN_16727 | 90550 | CCDC109A | mitochondrial calcium uniporter | 0,9 | 2,6244 |
| ILMN_22255 | 27034 | ACAD8 | acyl-CoA dehydrogenase family, memb | 0,9 | 1,2499 |
| ILMN_17163 | 64225 | ATL2 | atlastin GTPase 2 | 0,9 | 1,2499 |
| ILMN_17553 | 7275 | TUB | tubby homolog (mouse) | 0,9 | 0,8244 |
| ILMN_16573 | 5439 | POLR2J | polymerase (RNA) II (DNA directed) pol | 0,9 | 2,0799 |
| ILMN_21148 | 6135 | RPL11 | ribosomal protein L11 | 0,9 | 2,6244 |
| ILMN_32483 | 54617 | INO80 | INO80 homolog (S. cerevisiae) | 0,9 | 1,2499 |
| ILMN_18067 | 140459 | ASB6 | ankyrin repeat and SOCS box containing | 0,9 | 2,6244 |
| ILMN_16542 | 115 | ADCY9 | adenylate cyclase 9 | 0,9 | 1,2499 |
| ILMN_17308 | 284424 | C19orf30 | MIR7-3 host gene (non-protein coding) | 0,9 | 2,0799 |

| | | | | | |
|---|---|---|---|---|---|
| ILMN_17267( | 55748 | CNDP2 | CNDP dipeptidase 2 (metallopeptidase | 0,9 | 1,5007 |
| ILMN_17128( | 126669 | SHE | Src homology 2 domain containing E | 0,9 | 2,0799 |
| ILMN_17751( | 5136 | PDE1A | phosphodiesterase 1A, calmodulin-dep | 0,9 | 2,6244 |
| ILMN_18123( | 9168 | TMSB10 | thymosin beta 10 | 0,9 | 1,8141 |
| ILMN_17047( | 22918 | CD93 | CD93 molecule | 0,9 | 1,5007 |
| ILMN_16759( | 3459 | IFNGR1 | interferon gamma receptor 1 | 0,9 | 1,8141 |
| ILMN_16851( | 54942 | C9orf6 | family with sequence similarity 206, me | 0,9 | 2,0799 |
| ILMN_17041( | 207063 | DHRSX | dehydrogenase/reductase (SDR family) | 0,9 | 1,5007 |
| ILMN_17901( | 3815 | KIT | v-kit Hardy-Zuckerman 4 feline sarcoma | 0,9 | 2,6244 |
| ILMN_16886( | 10782 | ZNF274 | zinc finger protein 274 | 0,9 | 1,2499 |
| ILMN_17601( | 6804 | STX1A | syntaxin 1A (brain) | 0,9 | 1,8141 |
| ILMN_16731( | 79042 | TSEN34 | tRNA splicing endonuclease 34 homolog | 0,9 | 2,6244 |
| ILMN_17738( | 7041 | TGFB1I1 | transforming growth factor beta 1 indu | 0,9 | 2,6244 |
| ILMN_17244( | 23464 | GCAT | glycine C-acetyltransferase | 0,9 | 2,0799 |
| ILMN_17076( | 10686 | CLDN16 | claudin 16 | 0,9 | 1,8141 |

e)

**Supplemental Figure 2**

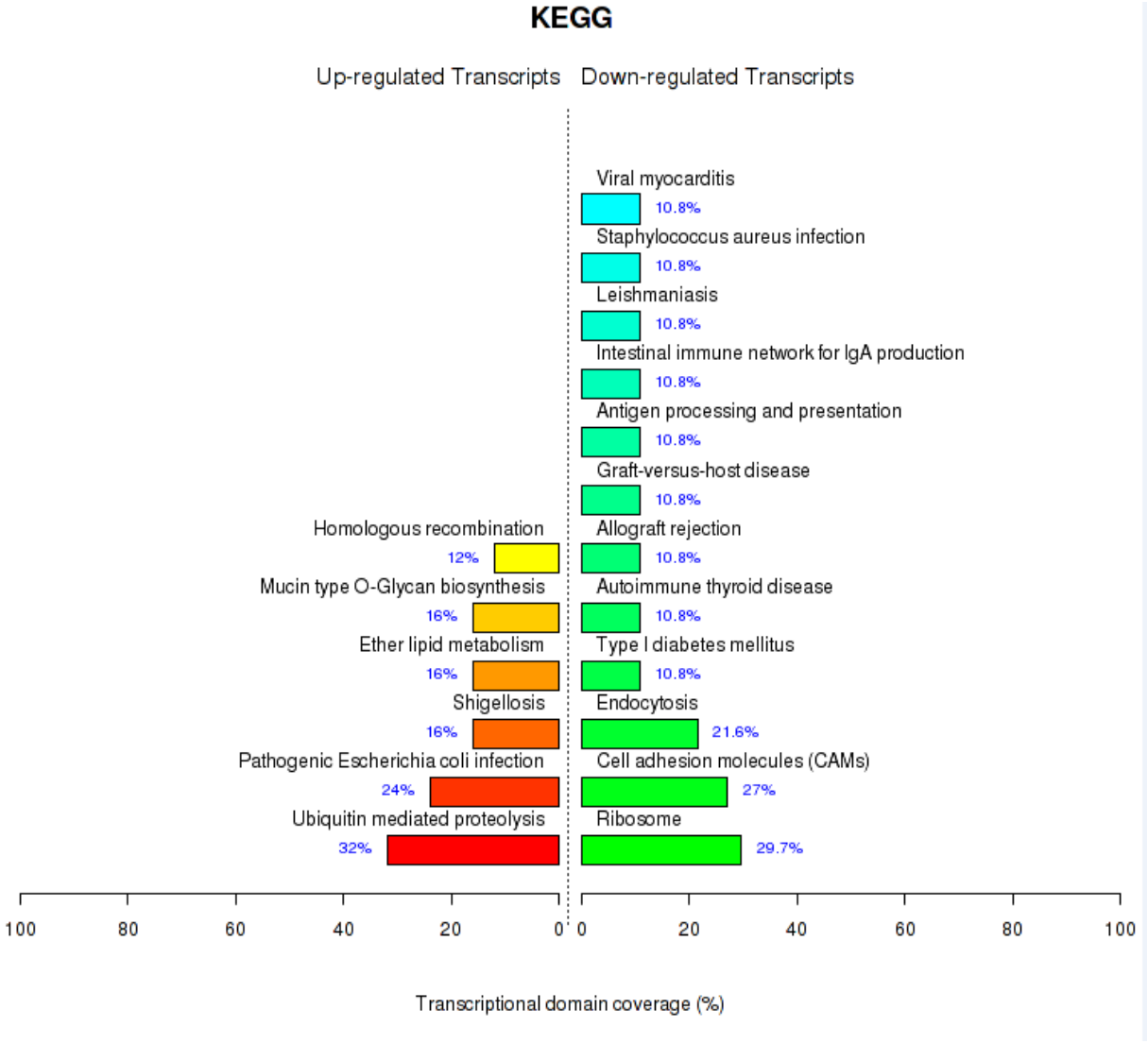

**Supplemental Figure 1**

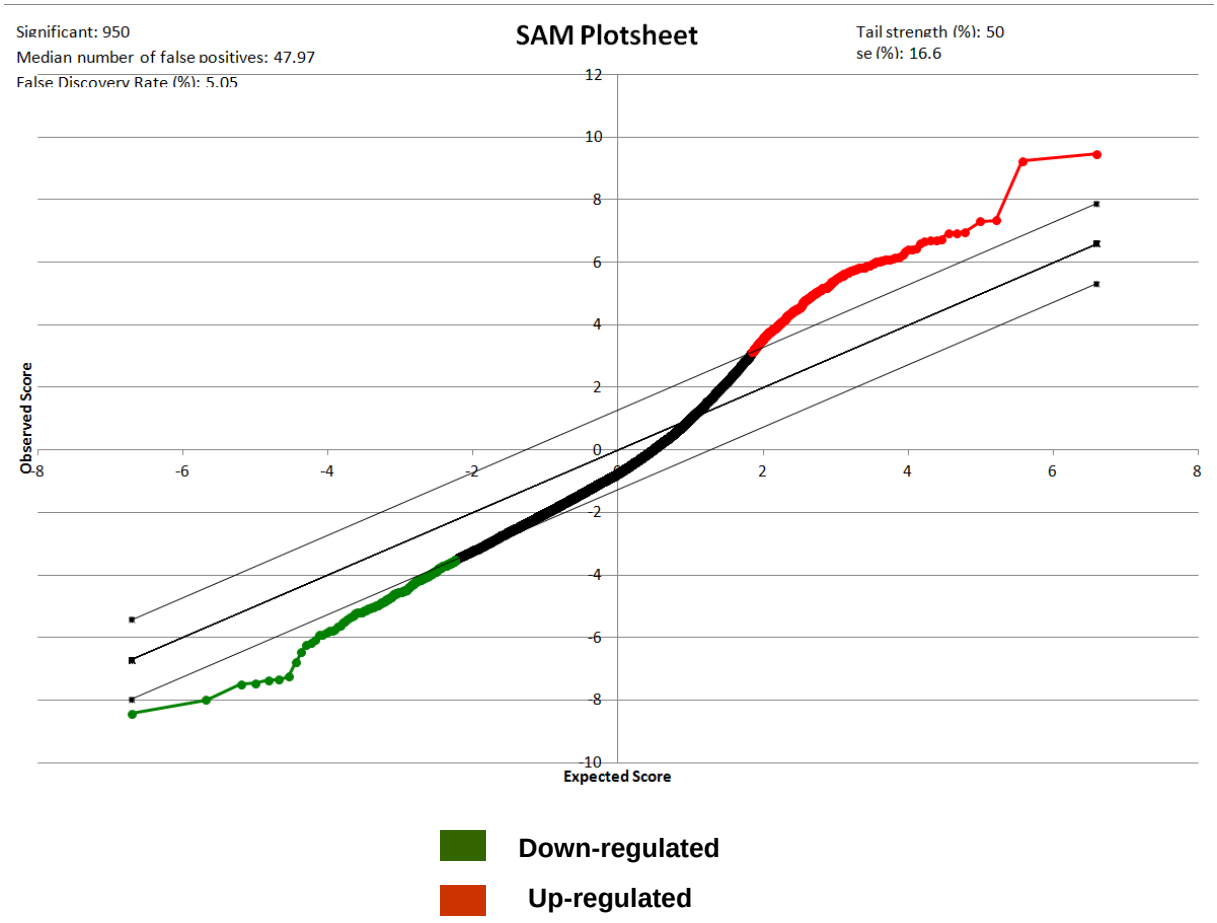

| Gene ID | ID | Gene ID | NAME | Fold Chang | p-value(% |
|---|---|---|---|---|---|
| ILMN_20753 | 8364 | HIST1H4C | histone cluster 1, H4c | 10,6 | 1,8141 |
| ILMN_32514 | 64710 | NUCKS1 | nuclear casein kinase and cyclin-depen | 8,6 | 1,0331 |
| ILMN_21135 | 51449 | PCYOX1 | prenylcysteine oxidase 1 | 7,7 | 1,5007 |
| ILMN_21300 | 91368 | CDKN2AIPNL | CDKN2A interacting protein N-terminal | 7,7 | 0,3847 |
| ILMN_16613 | 6711 | SPTBN1 | spectrin, beta, non-erythrocytic 1 | 6,8 | 1,5007 |
| ILMN_21159 | 84124 | ZNF394 | zinc finger protein 394 | 6,3 | 1,8141 |
| ILMN_24157 | 26118 | WSB1 | WD repeat and SOCS box containing 1 | 6,3 | 1,2499 |
| ILMN_20519 | 126272 | EID2B | EP300 interacting inhibitor of different | 6,1 | 1,2499 |
| ILMN_21137 | 157777 | C8orf45 | minichromosome maintenance domair | 6,0 | 0,3847 |
| ILMN_32371 | 84142 | FAM175A | family with sequence similarity 175, me | 6,0 | 0,6097 |
| ILMN_22274 | 256051 | ZNF549 | zinc finger protein 549 | 5,9 | 1,5007 |
| ILMN_16921 | 7561 | ZNF14 | zinc finger protein 14 | 5,8 | 0,3847 |
| ILMN_23138 | 91120 | ZNF682 | zinc finger protein 682 | 5,7 | 0,7969 |
| ILMN_21768 | 7620 | ZNF69 | zinc finger protein 69 | 5,7 | 1,8141 |
| ILMN_21502 | 55033 | FKBP14 | FK506 binding protein 14, 22 kDa | 5,7 | 1,5007 |
| ILMN_22103 | 200728 | TMEM17 | transmembrane protein 17 | 5,6 | 1,8141 |
| ILMN_21107 | 1138 | CHRNA5 | cholinergic receptor, nicotinic, alpha 5 | 5,6 | 1,5007 |
| ILMN_17224 | 142679 | DUSP19 | dual specificity phosphatase 19 | 5,6 | 1,8141 |
| ILMN_22860 | 117155 | CATSPER2 | cation channel, sperm associated 2 | 5,5 | 0,3847 |
| ILMN_22153 | 317781 | DDX51 | DEAD (Asp-Glu-Ala-Asp) box polypeptic | 5,5 | 0,3847 |
| ILMN_17350 | 1316 | KLF6 | Kruppel-like factor 6 | 5,5 | 1,5007 |
| ILMN_32416 | 84109 | QRFPR | pyroglutamylated RFamide peptide rec | 5,5 | 0,7969 |
| ILMN_21225 | 147372 | CCBE1 | collagen and calcium binding EGF dom | 5,4 | 0,3847 |
| ILMN_16615 | 54741 | LEPROT | leptin receptor overlapping transcript | 5,4 | 0,6097 |
| ILMN_21881 | 339231 | ARL16 | ADP-ribosylation factor-like 16 | 5,3 | 0,3847 |
| ILMN_17213 | 84061 | MAGT1 | magnesium transporter 1 | 5,3 | 1,0331 |
| ILMN_32381 | 399761 | BMS1P5 | BMS1 pseudogene 5 | 5,3 | 0,7969 |
| ILMN_22061 | 57477 | SHROOM4 | shroom family member 4 | 5,2 | 1,8141 |
| ILMN_22357 | 56850 | GRIPAP1 | GRIP1 associated protein 1 | 5,1 | 1,0331 |
| ILMN_22049 | 7516 | XRCC2 | X-ray repair complementing defective r | 5,0 | 1,5007 |
| ILMN_23342 | 1385 | CREB1 | cAMP responsive element binding prot | 5,0 | 1,2499 |
| ILMN_22857 | 55775 | TDP1 | tyrosyl-DNA phosphodiesterase 1 | 5,0 | 1,8141 |
| ILMN_21543 | 9723 | SEMA3E | sema domain, immunoglobulin domair | 4,9 | 2,0799 |
| ILMN_22357 | 81033 | KCNH6 | potassium voltage-gated channel, subf | 4,9 | 0,3847 |
| ILMN_17510 | 162073 | ITPRIPL2 | inositol 1,4,5-trisphosphate receptor in | 4,9 | 1,0331 |
| ILMN_22301 | 641737 | FLJ44124 | uncharacterized LOC641737 | 4,9 | 0,3847 |
| ILMN_17857 | 56203 | LMOD3 | leiomodin 3 (fetal) | 4,8 | 1,5007 |
| ILMN_20787 | 84334 | C14orf153 | apoptogenic 1 | 4,8 | 1,2499 |
| ILMN_17104 | 5700 | PSMC1 | proteasome (prosome, macropain) 26S | 4,8 | 0,7969 |
| ILMN_20785 | 154791 | HSPC268 | chromosome 7 open reading frame 55 | 4,7 | 1,0331 |
| ILMN_21623 | 11144 | DMC1 | DMC1 dosage suppressor of mck1 hom | 4,7 | 1,5007 |
| ILMN_21948 | 649598 | FLJ46309 | hypothetical protein LOC649598 | 4,7 | 0,3847 |
| ILMN_21284 | 1601 | DAB2 | disabled homolog 2, mitogen-responsiv | 4,7 | 1,5007 |
| ILMN_21233 | 64167 | LRAP | endoplasmic reticulum aminopeptidase | 4,7 | 1,2499 |
| ILMN_21175 | 64789 | DEM1 | defects in morphology 1 homolog (S. ce | 4,7 | 1,2499 |

| | | | | | |
|---|---|---|---|---|---|
| ILMN_20757 | 126205 | NLRP8 | NLR family, pyrin domain containing 8 | 4,7 | 0,3847 |
| ILMN_17724 | 92014 | MCART1 | solute carrier family 25, member 51 | 4,6 | 0,3847 |
| ILMN_17360 | 79693 | YRDC | yrdC domain containing (E. coli) | 4,5 | 0,7969 |
| ILMN_16914 | 5718 | PSMD12 | proteasome (prosome, macropain) 26S | 4,5 | 0,6097 |
| ILMN_16797 | 51449 | PCYOX1 | prenylcysteine oxidase 1 | 4,4 | 1,5007 |
| ILMN_20911 | 80867 | HCG2P7 | HLA complex group 2 pseudogene 7 | 4,3 | 1,2499 |
| ILMN_21397 | 22998 | LIMCH1 | LIM and calponin homology domains 1 | 4,3 | 1,5007 |
| ILMN_20493 | 151194 | FAM119A | methyltransferase like 21A | 4,2 | 1,2499 |
| ILMN_23611 | 64393 | ZMAT3 | zinc finger, matrin-type 3 | 4,2 | 1,5007 |
| ILMN_17374 | 1316 | KLF6 | Kruppel-like factor 6 | 4,2 | 2,0799 |
| ILMN_16802 | 25862 | USP49 | ubiquitin specific peptidase 49 | 4,1 | 0,3847 |
| ILMN_32354 | 84278 | HIATL2 | hippocampus abundant transcript-like | 4,1 | 1,0331 |
| ILMN_20735 | 25764 | C15orf63 | chromosome 15 open reading frame 63 | 4,1 | 1,2499 |
| ILMN_21178 | 503632 | DUXAP3 | double homeobox A pseudogene 3 | 4,1 | 1,0331 |
| ILMN_21504 | 64417 | C5orf28 | chromosome 5 open reading frame 28 | 4,1 | 1,2499 |
| ILMN_22798 | 158399 | ZNF483 | zinc finger protein 483 | 4,1 | 1,5007 |
| ILMN_24078 | 54756 | IL17RD | interleukin 17 receptor D | 4,0 | 0,7969 |
| ILMN_21066 | 8548 | BLZF1 | basic leucine zipper nuclear factor 1 | 4,0 | 1,5007 |
| ILMN_32456 | 147172 | LRRC37B2 | leucine rich repeat containing 37B pseu | 4,0 | 1,0331 |
| ILMN_16801 | 10087 | COL4A3BP | collagen, type IV, alpha 3 (Goodpasture | 4,0 | 1,2499 |
| ILMN_32251 | 148203 | ZNF738 | zinc finger protein 738 | 4,0 | 1,0331 |
| ILMN_22793 | 2204 | FCAR | Fc fragment of IgA, receptor for | 4,0 | 2,6244 |
| ILMN_22494 | 10558 | SPTLC1 | serine palmitoyltransferase, long chain | 4,0 | 0,3847 |
| ILMN_16937 | 250 | ALPP | alkaline phosphatase, placental | 3,9 | 1,2499 |
| ILMN_16817 | 2309 | FOXO3 | forkhead box O3 | 3,9 | 1,8141 |
| ILMN_32443 | 202243 | CCDC125 | coiled-coil domain containing 125 | 3,9 | 0,6097 |
| ILMN_24011 | 9698 | PUM1 | pumilio homolog 1 (Drosophila) | 3,9 | 1,2499 |
| ILMN_22767 | 23509 | POFUT1 | protein O-fucosyltransferase 1 | 3,9 | 1,8141 |
| ILMN_23701 | 3192 | HNRNPU | heterogeneous nuclear ribonucleoprot | 3,8 | 1,2499 |
| ILMN_17449 | 22836 | RHOBTB3 | Rho-related BTB domain containing 3 | 3,8 | 1,5007 |
| ILMN_18121 | 8396 | PIP5K2B | phosphatidylinositol-5-phosphate 4-kir | 3,7 | 0,3847 |
| ILMN_21066 | 8548 | BLZF1 | basic leucine zipper nuclear factor 1 | 3,7 | 0,7969 |
| ILMN_32363 | 205327 | C2orf69 | chromosome 2 open reading frame 69 | 3,7 | 0,7969 |
| ILMN_23815 | 27297 | CRCP | CGRP receptor component | 3,7 | 0,3847 |
| ILMN_22117 | 400866 | C21orf24 | long intergenic non-protein coding RNA | 3,6 | 1,2499 |
| ILMN_20591 | 79939 | SLC35E1 | solute carrier family 35, member E1 | 3,6 | 0,3847 |
| ILMN_18141 | 6925 | TCF4 | transcription factor 4 | 3,6 | 1,2499 |
| ILMN_16716 | 51478 | HSD17B7 | hydroxysteroid (17-beta) dehydrogena | 3,6 | 1,2499 |
| ILMN_17985 | 84515 | MCM8 | minichromosome maintenance comple | 3,6 | 0,3847 |
| ILMN_16977 | 55333 | SYNJ2BP | synaptojanin 2 binding protein | 3,6 | 1,2499 |
| ILMN_20545 | 285605 | DTWD2 | DTW domain containing 2 | 3,6 | 0,3847 |
| ILMN_33078 | 54058 | C21orf58 | chromosome 21 open reading frame 58 | 3,5 | 0,6097 |
| ILMN_16894 | 26137 | ZBTB20 | zinc finger and BTB domain containing | 3,5 | 1,0331 |
| ILMN_21235 | 374986 | FAM73A | family with sequence similarity 73, mer | 3,5 | 0,3847 |
| ILMN_23342 | 1385 | CREB1 | cAMP responsive element binding prot | 3,5 | 0,6097 |
| ILMN_20549 | 63929 | XPNPEP3 | X-prolyl aminopeptidase (aminopeptid | 3,4 | 1,5007 |

| | | | | | |
|---|---|---|---|---|---|
| ILMN_23304 | 54940 | OCIAD1 | OCIA domain containing 1 | 3,4 | 0,3847 |
| ILMN_22128 | 84765 | ZNF577 | zinc finger protein 577 | 3,4 | 1,5007 |
| ILMN_20790 | 58493 | C9orf80 | chromosome 9 open reading frame 80 | 3,4 | 0,6097 |
| ILMN_23424 | 27068 | PPA2 | pyrophosphatase (inorganic) 2 | 3,3 | 0,3847 |
| ILMN_20910 | 157657 | C8orf37 | chromosome 8 open reading frame 37 | 3,3 | 0,3847 |
| ILMN_22884 | 84984 | C3orf34 | centrosomal protein 19kDa | 3,3 | 1,5007 |
| ILMN_22622 | 10206 | TRIM13 | tripartite motif containing 13 | 3,3 | 1,5007 |
| ILMN_21581 | 80264 | ZNF430 | zinc finger protein 430 | 3,3 | 0,7969 |
| ILMN_16980 | 10395 | DLC1 | deleted in liver cancer 1 | 3,3 | 1,0331 |
| ILMN_16719 | 7360 | UGP2 | UDP-glucose pyrophosphorylase 2 | 3,2 | 0,7969 |
| ILMN_21553 | 22834 | ZNF652 | zinc finger protein 652 | 3,2 | 0,3847 |
| ILMN_17267 | 246243 | RNASEH1 | ribonuclease H1 | 3,2 | 2,0799 |
| ILMN_32517 | 87178 | PNPT1 | polyribonucleotide nucleotidyltransfer | 3,2 | 0,7969 |
| ILMN_16559 | 9701 | SAPS2 | protein phosphatase 6, regulatory subu | 3,1 | 1,8141 |
| ILMN_20733 | 3586 | IL10 | interleukin 10 | 3,1 | 0,3847 |
| ILMN_32492 | 113277 | TMEM106A | transmembrane protein 106A | 3,1 | 0,3847 |
| ILMN_18126 | 4641 | MYO1C | myosin IC | 3,1 | 0,3847 |
| ILMN_21809 | 387700 | SLC16A12 | solute carrier family 16, member 12 (m | 3,1 | 0,3847 |
| ILMN_22435 | 10838 | ZNF275 | zinc finger protein 275 | 3,0 | 0,3847 |
| ILMN_16615 | 977 | CD151 | CD151 molecule (Raph blood group) | 3,0 | 0,7969 |
| ILMN_21052 | 145482 | PTGR2 | prostaglandin reductase 2 | 3,0 | 0,3847 |
| ILMN_21689 | 8562 | DENR | density-regulated protein | 3,0 | 0,6097 |
| ILMN_17782 | 285966 | FLJ40722 | family with sequence similarity 115, me | 3,0 | 0,3847 |
| ILMN_17863 | 3842 | TNPO1 | transportin 1 | 3,0 | 2,6244 |
| ILMN_20535 | 54933 | RHBDL2 | rhomboid, veinlet-like 2 (Drosophila) | 2,9 | 0,3847 |
| ILMN_18056 | 90649 | ZNF486 | zinc finger protein 486 | 2,9 | 0,3847 |
| ILMN_22221 | 55728 | N4BP2 | NEDD4 binding protein 2 | 2,9 | 0,3847 |
| ILMN_20553 | 8930 | MBD4 | methyl-CpG binding domain protein 4 | 2,9 | 1,2499 |
| ILMN_32450 | 50807 | ASAP1 | ArfGAP with SH3 domain, ankyrin repe | 2,8 | 1,8141 |
| ILMN_17137 | 136051 | ZNF786 | zinc finger protein 786 | 2,8 | 0,3847 |
| ILMN_23974 | 10052 | GJC1 | gap junction protein, gamma 1, 45kDa | 2,8 | 0,7969 |
| ILMN_16943 | 3382 | ICA1 | islet cell autoantigen 1, 69kDa | 2,8 | 0,3847 |
| ILMN_17636 | 89970 | RSPRY1 | ring finger and SPRY domain containing | 2,8 | 1,8141 |
| ILMN_32266 | 642280 | MGC26356 | zinc finger protein 876, pseudogene | 2,8 | 0,7969 |
| ILMN_16810 | 10555 | AGPAT2 | 1-acylglycerol-3-phosphate O-acyltrans | 2,7 | 1,8141 |
| ILMN_16919 | 10983 | CCNI | cyclin I | 2,7 | 1,0331 |
| ILMN_17612 | 5143 | PDE4C | phosphodiesterase 4C, cAMP-specific | 2,7 | 0,3847 |
| ILMN_17212 | 1438 | CSF2RA | colony stimulating factor 2 receptor, al | 2,7 | 0,3847 |
| ILMN_23633 | 8740 | TNFSF14 | tumor necrosis factor (ligand) superfan | 2,7 | 1,0331 |
| ILMN_23831 | 27072 | VPS41 | vacuolar protein sorting 41 homolog (S | 2,7 | 0,3847 |
| ILMN_21050 | 26258 | PLDN | pallidin homolog (mouse) | 2,6 | 0,3847 |
| ILMN_16670 | 55066 | PDPR | pyruvate dehydrogenase phosphatase | 2,6 | 1,8141 |
| ILMN_20891 | 94056 | SYAP1 | synapse associated protein 1 | 2,6 | 0,3847 |
| ILMN_16901 | 401494 | PTPLAD2 | protein tyrosine phosphatase-like A do | 2,6 | 0,3847 |
| ILMN_16590 | 9475 | ROCK2 | Rho-associated, coiled-coil containing p | 2,6 | 1,5007 |
| ILMN_24056 | 330 | BIRC3 | baculoviral IAP repeat containing 3 | 2,6 | 1,5007 |

| | | | | | |
|---|---|---|---|---|---|
| ILMN_32516( | 54813 | KLHL28 | kelch-like 28 (Drosophila) | 2,6 | 1,0331 |
| ILMN_17110 | 653489 | LOC653489 | RANBP2-like and GRIP domain containi | 2,5 | 0,7969 |
| ILMN_18085( | 30011 | SH3KBP1 | SH3-domain kinase binding protein 1 | 2,5 | 1,8141 |
| ILMN_20514( | 87178 | PNPT1 | polyribonucleotide nucleotidyltransfer | 2,5 | 0,6097 |
| ILMN_21750 | 56165 | TDRD1 | tudor domain containing 1 | 2,5 | 2,0799 |
| ILMN_18142( | 54943 | C21orf55 | DnaJ (Hsp40) homolog, subfamily C, me | 2,5 | 0,7969 |
| ILMN_22435 | 79864 | C11orf63 | chromosome 11 open reading frame 63 | 2,5 | 0,3847 |
| ILMN_23169 | 10859 | LILRB1 | leukocyte immunoglobulin-like receptc | 2,4 | 1,0331 |
| ILMN_23764 | 1438 | CSF2RA | colony stimulating factor 2 receptor, al | 2,4 | 0,6097 |
| ILMN_32402 | 140771 | SMCR5 | Smith-Magenis syndrome chromosome | 2,4 | 0,3847 |
| ILMN_17306 | 374860 | ANKRD30B | ankyrin repeat domain 30B | 2,4 | 1,0331 |
| ILMN_17784 | 3606 | IL18 | interleukin 18 (interferon-gamma-indu | 2,4 | 1,0331 |
| ILMN_22203 | 285855 | RPL7L1 | ribosomal protein L7-like 1 | 2,4 | 0,7969 |
| ILMN_17367( | 226 | ALDOA | aldolase A, fructose-bisphosphate | 2,4 | 2,6244 |
| ILMN_21610( | 126626 | GABPB2 | GA binding protein transcription factor | 2,4 | 0,7969 |
| ILMN_24019( | 146059 | CDAN1 | codanin 1 | 2,4 | 0,6097 |
| ILMN_22281 | 221322 | C6orf170 | chromosome 6 open reading frame 17( | 2,4 | 0,7969 |
| ILMN_18131( | 117248 | GALNTL2 | UDP-N-acetyl-alpha-D-galactosamine:p | 2,4 | 2,6244 |
| ILMN_18155 | 7766 | ZNF223 | zinc finger protein 223 | 2,3 | 0,3847 |
| ILMN_21016 | 54799 | MBTD1 | mbt domain containing 1 | 2,3 | 2,6244 |
| ILMN_16914 | 4826 | NNAT | neuronatin | 2,3 | 2,0799 |
| ILMN_21612 | 57464 | FAM40B | family with sequence similarity 40, mer | 2,3 | 0,3847 |
| ILMN_21063 | 9966 | TNFSF15 | tumor necrosis factor (ligand) superfan | 2,3 | 1,5007 |
| ILMN_21522 | 6752 | SSTR2 | somatostatin receptor 2 | 2,3 | 1,2499 |
| ILMN_22732 | 57835 | SLC4A5 | solute carrier family 4, sodium bicarbor | 2,3 | 0,3847 |
| ILMN_24047 | 6817 | SULT1A1 | sulfotransferase family, cytosolic, 1A, p | 2,3 | 0,0000 |
| ILMN_18039 | 286451 | YIPF6 | Yip1 domain family, member 6 | 2,3 | 1,2499 |
| ILMN_32601 | 401082 | FLJ25363 | uncharacterized LOC401082 | 2,3 | 0,7969 |
| ILMN_20937 | 79862 | ZNF669 | zinc finger protein 669 | 2,3 | 0,3847 |
| ILMN_16534 | 84839 | RAXL1 | retina and anterior neural fold homeob | 2,2 | 0,3847 |
| ILMN_17451 | 23543 | RBM9 | RNA binding protein, fox-1 homolog (C | 2,2 | 1,5007 |
| ILMN_17601 | 64121 | RRAGC | Ras-related GTP binding C | 2,2 | 1,2499 |
| ILMN_22249( | 201895 | C4orf34 | chromosome 4 open reading frame 34 | 2,2 | 1,8141 |
| ILMN_22099 | 440503 | PLIN5 | perilipin 5 | 2,2 | 0,3847 |
| ILMN_17384 | 55142 | CEP27 | HAUS augmin-like complex, subunit 2 | 2,2 | 0,7969 |
| ILMN_20974 | 27071 | DAPP1 | dual adaptor of phosphotyrosine and 3 | 2,2 | 0,6097 |
| ILMN_21062( | 284161 | GDPD1 | glycerophosphodiester phosphodieste | 2,2 | 1,5007 |
| ILMN_17811 | 4067 | LYN | v-yes-1 Yamaguchi sarcoma viral relate | 2,2 | 1,8141 |
| ILMN_22330 | 26279 | PLA2G2D | phospholipase A2, group IID | 2,2 | 0,3847 |
| ILMN_22615 | 326 | AIRE | autoimmune regulator | 2,2 | 0,7969 |
| ILMN_20933 | 6617 | SNAPC1 | small nuclear RNA activating complex, | 2,2 | 1,0331 |
| ILMN_16884 | 8073 | PTP4A2 | protein tyrosine phosphatase type IVA, | 2,2 | 0,3847 |
| ILMN_20488 | 80224 | NUBPL | nucleotide binding protein-like | 2,1 | 0,3847 |
| ILMN_16766( | 404093 | CUEDC1 | CUE domain containing 1 | 2,1 | 0,7969 |
| ILMN_17673 | 367 | AR | androgen receptor | 2,1 | 1,5007 |
| ILMN_18112 | 160728 | SLC5A8 | solute carrier family 5 (iodide transport | 2,1 | 0,3847 |

| | | | | | |
|---|---|---|---|---|---|
| ILMN_22841 | 7360 | UGP2 | UDP-glucose pyrophosphorylase 2 | 2,1 | 2,6244 |
| ILMN_16562 | 79827 | ASAM | CXADR-like membrane protein | 2,1 | 2,0799 |
| ILMN_18140 | 5256 | PHKA2 | phosphorylase kinase, alpha 2 (liver) | 2,1 | 0,6097 |
| ILMN_17872 | 84858 | ZNF503 | zinc finger protein 503 | 2,1 | 2,6244 |
| ILMN_20478 | 56127 | PCDHB9 | protocadherin beta 9 | 2,1 | 0,3847 |
| ILMN_22465 | 653399 | GSTTP2 | glutathione S-transferase theta pseudc | 2,1 | 0,7969 |
| ILMN_20700 | 152926 | PPM1K | protein phosphatase, Mg2+/Mn2+ dep | 2,1 | 1,2499 |
| ILMN_23573 | 2218 | FKTN | fukutin | 2,1 | 0,7969 |
| ILMN_18010 | 6693 | SPN | sialophorin | 2,0 | 2,0799 |
| ILMN_32393 | 442578 | STAG3L3 | stromal antigen 3-like 3 | 2,0 | 1,5007 |
| ILMN_20969 | 140469 | MYO3B | myosin IIIB | 2,0 | 1,5007 |
| ILMN_16760 | 22982 | DIP2C | DIP2 disco-interacting protein 2 homol | 2,0 | 2,6244 |
| ILMN_18126 | 196 | AHR | aryl hydrocarbon receptor | 2,0 | 0,7969 |
| ILMN_16957 | 27161 | EIF2C2 | eukaryotic translation initiation factor | 2,0 | 2,0799 |
| ILMN_32464 | 3187 | HNRNPH1 | heterogeneous nuclear ribonucleoprot | 2,0 | 0,7969 |
| ILMN_22970 | 9747 | FAM115A | family with sequence similarity 115, me | 2,0 | 1,5007 |
| ILMN_17561 | 79157 | MFSD11 | major facilitator superfamily domain co | 2,0 | 1,2499 |
| ILMN_17267 | 23112 | TNRC6B | trinucleotide repeat containing 6B | 2,0 | 0,3847 |
| ILMN_22609 | 706 | TSPO | translocator protein (18kDa) | 2,0 | 1,8141 |
| ILMN_17551 | 440275 | EIF2AK4 | eukaryotic translation initiation factor | 2,0 | 0,3847 |
| ILMN_17463 | 7813 | EVI5 | ecotropic viral integration site 5 | 2,0 | 1,0331 |
| ILMN_18061 | 57680 | CHD8 | chromodomain helicase DNA binding p | 2,0 | 1,2499 |
| ILMN_17975 | 1845 | DUSP3 | dual specificity phosphatase 3 | 2,0 | 1,8141 |
| ILMN_23219 | 64421 | DCLRE1C | DNA cross-link repair 1C | 2,0 | 0,3847 |
| ILMN_24061 | 11025 | LILRB3 | leukocyte immunoglobulin-like receptc | 2,0 | 0,7969 |
| ILMN_22747 | 80736 | SLC44A4 | solute carrier family 44, member 4 | 2,0 | 1,2499 |
| ILMN_23240 | 800 | CALD1 | caldesmon 1 | 1,9 | 1,8141 |
| ILMN_16893 | 9891 | NUAK1 | NUAK family, SNF1-like kinase, 1 | 1,9 | 1,2499 |
| ILMN_17913 | 442582 | STAG3L2 | stromal antigen 3-like 2 | 1,9 | 1,2499 |
| ILMN_17080 | 4134 | MAP4 | microtubule-associated protein 4 | 1,9 | 0,3847 |
| ILMN_23522 | 166824 | RASSF6 | Ras association (RalGDS/AF-6) domain | 1,9 | 0,7969 |
| ILMN_17770 | 90338 | ZNF160 | zinc finger protein 160 | 1,9 | 0,3847 |
| ILMN_32392 | 6085 | RNY3 | RNA, Ro-associated Y3 | 1,9 | 0,6097 |
| ILMN_21482 | 10081 | PDCD7 | programmed cell death 7 | 1,9 | 1,2499 |
| ILMN_18150 | 5292 | PIM1 | pim-1 oncogene | 1,9 | 1,8141 |
| ILMN_17956 | 8073 | PTP4A2 | protein tyrosine phosphatase type IVA, | 1,9 | 1,8141 |
| ILMN_17146 | 27327 | TNRC6A | trinucleotide repeat containing 6A | 1,9 | 1,2499 |
| ILMN_21824 | 79801 | SHCBP1 | SHC SH2-domain binding protein 1 | 1,9 | 1,0331 |
| ILMN_18156 | 10955 | SERINC3 | serine incorporator 3 | 1,9 | 1,2499 |
| ILMN_32285 | 84222 | TMEM191A | transmembrane protein 191A (pseudo | 1,9 | 0,3847 |
| ILMN_32696 | 255031 | FLJ35390 | uncharacterized LOC255031 | 1,9 | 0,3847 |
| ILMN_17891 | 3652 | IPP | intracisternal A particle-promoted poly | 1,9 | 0,7969 |
| ILMN_17217 | 5469 | PPARBP | mediator complex subunit 1 | 1,9 | 2,0799 |
| ILMN_17590 | 115509 | ZNF689 | zinc finger protein 689 | 1,9 | 2,6244 |
| ILMN_17220 | 55156 | ARMC1 | armadillo repeat containing 1 | 1,9 | 2,0799 |
| ILMN_20646 | 91966 | CXorf40A | chromosome X open reading frame 40 | 1,9 | 2,0799 |

| | | | | | |
|---|---|---|---|---|---|
| ILMN_17536 | 3202 | HOXA5 | homeobox A5 | 1,9 | 0,3847 |
| ILMN_16904 | 145438 | C14orf82 | FRMD6 antisense RNA 1 (non-protein c | 1,8 | 0,3847 |
| ILMN_17523 | 79939 | SLC35E1 | solute carrier family 35, member E1 | 1,8 | 2,0799 |
| ILMN_16913 | 6772 | STAT1 | signal transducer and activator of trans | 1,8 | 2,0799 |
| ILMN_23962 | 27250 | PDCD4 | programmed cell death 4 (neoplastic tr | 1,8 | 0,7969 |
| ILMN_23360 | 55714 | ODZ3 | odz, odd Oz/ten-m homolog 3 (Drosopl | 1,8 | 2,6244 |
| ILMN_17489 | 83734 | ATG10 | autophagy related 10 | 1,8 | 1,8141 |
| ILMN_22259 | 2730 | GCLM | glutamate-cysteine ligase, modifier sub | 1,8 | 1,2499 |
| ILMN_17656 | 10056 | FARSLB | phenylalanyl-tRNA synthetase, beta sul | 1,8 | 1,0331 |
| ILMN_23514 | 50863 | NTM | neurotrimin | 1,8 | 1,8141 |
| ILMN_17386 | 286354 | C9orf130 | chromosome 9 open reading frame 130 | 1,8 | 0,7969 |
| ILMN_23461 | 79230 | ZNF557 | zinc finger protein 557 | 1,8 | 0,3847 |
| ILMN_32266 | 11145 | PLA2G16 | phospholipase A2, group XVI | 1,8 | 2,0799 |
| ILMN_20926 | 124801 | LSM12 | LSM12 homolog (S. cerevisiae) | 1,8 | 1,8141 |
| ILMN_17031 | 57226 | LYRM2 | LYR motif containing 2 | 1,8 | 0,3847 |
| ILMN_17873 | 65068 | ALS2CR14 | amyotrophic lateral sclerosis 2 (juvenile | 1,8 | 0,3847 |
| ILMN_18094 | 10357 | HMGB1L1 | high mobility group box 1 pseudogene | 1,7 | 2,6244 |
| ILMN_18039 | 51768 | TM7SF3 | transmembrane 7 superfamily member | 1,7 | 1,5007 |
| ILMN_22708 | 54663 | WDR74 | WD repeat domain 74 | 1,7 | 1,0331 |
| ILMN_17026 | 84617 | TUBB6 | tubulin, beta 6 class V | 1,7 | 0,7969 |
| ILMN_21572 | 6718 | AKR1D1 | aldo-keto reductase family 1, member | 1,7 | 1,8141 |
| ILMN_17978 | 23512 | SUZ12 | suppressor of zeste 12 homolog (Drosc | 1,7 | 1,2499 |
| ILMN_16790 | 81931 | ZNF93 | zinc finger protein 93 | 1,7 | 0,3847 |
| ILMN_21754 | 54516 | MTRF1L | mitochondrial translational release fact | 1,7 | 0,7969 |
| ILMN_23626 | 8824 | CES2 | carboxylesterase 2 | 1,7 | 0,6097 |
| ILMN_17091 | 497262 | RUNDC2C | RUN domain containing 2C | 1,7 | 0,3847 |
| ILMN_23941 | 55471 | PRO1853 | chromosome 2 open reading frame 56 | 1,7 | 0,3847 |
| ILMN_16798 | 51186 | WBP5 | WW domain binding protein 5 | 1,7 | 0,7969 |
| ILMN_22194 | 79056 | PRRG4 | proline rich Gla (G-carboxyglutamic aci | 1,7 | 0,7969 |
| ILMN_23705 | 54739 | XAF1 | XIAP associated factor 1 | 1,7 | 1,5007 |
| ILMN_33067 | 54502 | RBM47 | RNA binding motif protein 47 | 1,7 | 1,2499 |
| ILMN_18155 | 3203 | HOXA6 | homeobox A6 | 1,7 | 0,7969 |
| ILMN_23937 | 10093 | ARPC4 | actin related protein 2/3 complex, subu | 1,7 | 2,0799 |
| ILMN_16575 | 91057 | CCDC34 | coiled-coil domain containing 34 | 1,7 | 1,0331 |
| ILMN_24144 | 5935 | RBM3 | RNA binding motif (RNP1, RRM) protein | 1,7 | 0,3847 |
| ILMN_21802 | 9980 | DOPEY2 | dopey family member 2 | 1,7 | 1,8141 |
| ILMN_21882 | 9140 | ATG12 | autophagy related 12 | 1,6 | 0,7969 |
| ILMN_16615 | 9729 | KIAA0408 | KIAA0408 | 1,6 | 1,0331 |
| ILMN_23876 | 1235 | CCR6 | chemokine (C-C motif) receptor 6 | 1,6 | 2,0799 |
| ILMN_33014 | 729324 | LOC729324 | hCG1986447 | 1,6 | 1,2499 |
| ILMN_24080 | 1936 | EEF1D | eukaryotic translation elongation facto | 1,6 | 2,6244 |
| ILMN_17092 | 81790 | RNF170 | ring finger protein 170 | 1,6 | 1,5007 |
| ILMN_20583 | 9475 | ROCK2 | Rho-associated, coiled-coil containing p | 1,6 | 1,8141 |
| ILMN_16853 | 374928 | ZNF773 | zinc finger protein 773 | 1,6 | 0,3847 |
| ILMN_22150 | 23594 | ORC6L | origin recognition complex, subunit 6 | 1,6 | 1,0331 |
| ILMN_20917 | 123688 | LOC123688 | aminoglycoside phosphotransferase do | 1,6 | 1,8141 |

| | | | | | |
|---|---|---|---|---|---|
| ILMN_17830( | 788 | SLC25A20 | solute carrier family 25 (carnitine/acylc | 1,6 | 0,3847 |
| ILMN_32453( | 344787 | ZNF860 | zinc finger protein 860 | 1,6 | 0,6097 |
| ILMN_17606( | 3200 | HOXA3 | homeobox A3 | 1,6 | 2,0799 |
| ILMN_21337( | 399967 | PATE2 | prostate and testis expressed 2 | 1,6 | 0,7969 |
| ILMN_23648( | 8473 | OGT | O-linked N-acetylglucosamine (GlcNAc) | 1,6 | 1,0331 |
| ILMN_17695( | 54965 | PIGX | phosphatidylinositol glycan anchor bios | 1,6 | 0,3847 |
| ILMN_16853( | 25870 | SUMF2 | sulfatase modifying factor 2 | 1,6 | 2,0799 |
| ILMN_23790( | 84901 | NFATC2IP | nuclear factor of activated T-cells, cyto | 1,6 | 0,3847 |
| ILMN_16833( | 6482 | ST3GAL1 | ST3 beta-galactoside alpha-2,3-sialyltra | 1,5 | 1,5007 |
| ILMN_16851( | 311 | ANXA11 | annexin A11 | 1,5 | 0,3847 |
| ILMN_16928( | 64718 | UNKL | unkempt homolog (Drosophila)-like | 1,5 | 1,5007 |
| ILMN_17312( | 57714 | RNF213 | KIAA1618 | 1,5 | 0,6097 |
| ILMN_17716( | 6629 | SNRPB2 | small nuclear ribonucleoprotein polype | 1,5 | 1,8141 |
| ILMN_16997( | 372 | ARCN1 | archain 1 | 1,5 | 1,8141 |
| ILMN_23630( | 5888 | RAD51 | RAD51 homolog (S. cerevisiae) | 1,5 | 0,3847 |
| ILMN_23655( | 7862 | BRPF1 | bromodomain and PHD finger containi | 1,5 | 0,3847 |
| ILMN_18029( | 51588 | PIAS4 | protein inhibitor of activated STAT, 4 | 1,5 | 0,3847 |
| ILMN_21847( | 150274 | HSCB | HscB iron-sulfur cluster co-chaperone h | 1,5 | 1,0331 |
| ILMN_16993( | 84820 | POLR2J4 | polymerase (RNA) II (DNA directed) pol | 1,5 | 0,0000 |
| ILMN_16525( | 29797 | DKFZp434K1 | POM121 transmembrane nucleoporin- | 1,5 | 0,7969 |
| ILMN_17398( | 54820 | NDE1 | nudE nuclear distribution E homolog 1 | 1,5 | 0,7969 |
| ILMN_33044( | 728640 | LOC728640 | family with sequence similarity 133, me | 1,5 | 0,3847 |
| ILMN_22054( | 202134 | FAM153B | family with sequence similarity 153, me | 1,5 | 2,0799 |
| ILMN_17676( | 25851 | TECPR1 | tectonin beta-propeller repeat contain | 1,5 | 0,7969 |
| ILMN_17757( | 55720 | TSR1 | TSR1, 20S rRNA accumulation, homolog | 1,5 | 0,7969 |
| ILMN_18119( | 27246 | ZNF364 | ring finger protein 115 | 1,5 | 0,7969 |
| ILMN_16988( | 51776 | ZAK | sterile alpha motif and leucine zipper c | 1,5 | 2,0799 |
| ILMN_18027( | 79647 | AKIRIN1 | akirin 1 | 1,5 | 1,8141 |
| ILMN_21304( | 10945 | KDELR1 | KDEL (Lys-Asp-Glu-Leu) endoplasmic re | 1,5 | 1,5007 |
| ILMN_17087( | 55766 | H2AFJ | H2A histone family, member J | 1,5 | 1,5007 |
| ILMN_17222( | 5048 | PAFAH1B1 | platelet-activating factor acetylhydrola | 1,5 | 2,0799 |
| ILMN_16815( | 5770 | PTPN1 | protein tyrosine phosphatase, non-rece | 1,5 | 1,0331 |
| ILMN_16902( | 84054 | PCDHB19P | protocadherin beta 19 pseudogene | 1,5 | 0,3847 |
| ILMN_17200( | 79618 | HMBOX1 | homeobox containing 1 | 1,5 | 1,2499 |
| ILMN_32377( | 55331 | ACER3 | alkaline ceramidase 3 | 1,5 | 0,3847 |
| ILMN_17458( | 57238 | KIAA0492 | KIAA0492 protein | 1,5 | 2,6244 |
| ILMN_16998( | 5900 | RALGDS | ral guanine nucleotide dissociation stin | 1,4 | 0,7969 |
| ILMN_17728( | 55893 | ZNF395 | zinc finger protein 395 | 1,4 | 0,7969 |
| ILMN_17369( | 7357 | UGCG | UDP-glucose ceramide glucosyltransfer | 1,4 | 2,0799 |
| ILMN_17619( | 6430 | SFRS5 | serine/arginine-rich splicing factor 5 | 1,4 | 1,2499 |
| ILMN_16614( | 10471 | PFDN6 | prefoldin subunit 6 | 1,4 | 1,0331 |
| ILMN_23944( | 283635 | FAM177A1 | family with sequence similarity 177, me | 1,4 | 2,0799 |
| ILMN_21432( | 541578 | CXorf40B | chromosome X open reading frame 40l | 1,4 | 2,6244 |
| ILMN_16710( | 2591 | GALNT3 | UDP-N-acetyl-alpha-D-galactosamine:p | 1,4 | 1,8141 |
| ILMN_17149( | 1629 | DBT | dihydrolipoamide branched chain trans | 1,4 | 1,2499 |
| ILMN_32420( | 493869 | GPX8 | glutathione peroxidase 8 (putative) | 1,4 | 1,0331 |

| | | | | | |
|---|---|---|---|---|---|
| ILMN_16982 | 5935 | RBM3 | RNA binding motif (RNP1, RRM) protei | 1,4 | 1,2499 |
| ILMN_32386 | 93556 | C3orf50 | EGF-like and EMI domain containing 1, | 1,4 | 1,8141 |
| ILMN_21019 | 3187 | HNRPH1 | heterogeneous nuclear ribonucleoprot | 1,4 | 0,6097 |
| ILMN_16558 | 57146 | TMEM159 | transmembrane protein 159 | 1,4 | 2,0799 |
| ILMN_16623 | 9406 | ZRANB2 | zinc finger, RAN-binding domain contai | 1,4 | 0,7969 |
| ILMN_20903 | 81875 | ISG20L2 | interferon stimulated exonuclease gen | 1,4 | 2,0799 |
| ILMN_17137 | 25 | ABL1 | c-abl oncogene 1, non-receptor tyrosin | 1,4 | 2,0799 |
| ILMN_20729 | 7156 | TOP3A | topoisomerase (DNA) III alpha | 1,4 | 1,2499 |
| ILMN_20956 | 80008 | TMEM156 | transmembrane protein 156 | 1,4 | 0,7969 |
| ILMN_32401 | 84298 | LLPH | LLP homolog, long-term synaptic facilit | 1,4 | 1,2499 |
| ILMN_17984 | 23254 | KIAA1026 | kazrin, periplakin interacting protein | 1,4 | 0,7969 |
| ILMN_16808 | 5965 | RECQL | RecQ protein-like (DNA helicase Q1-like | 1,4 | 0,3847 |
| ILMN_17881 | 5872 | RAB13 | RAB13, member RAS oncogene family | 1,4 | 1,5007 |
| ILMN_16784 | 162966 | ZNF600 | zinc finger protein 600 | 1,4 | 0,7969 |
| ILMN_16514 | 57222 | ERGIC1 | endoplasmic reticulum-golgi intermedi | 1,4 | 0,3847 |
| ILMN_16563 | 5523 | PPP2R3A | protein phosphatase 2, regulatory subu | 1,4 | 1,5007 |
| ILMN_17817 | 2079 | ERH | enhancer of rudimentary homolog (Dro | 1,4 | 2,6244 |
| ILMN_21972 | 11128 | POLR3A | polymerase (RNA) III (DNA directed) po | 1,4 | 1,5007 |
| ILMN_21234 | 656 | BMP8B | bone morphogenetic protein 8b | 1,4 | 0,3847 |
| ILMN_17628 | 9931 | HELZ | helicase with zinc finger | 1,4 | 2,0799 |
| ILMN_16828 | 8209 | C21orf33 | chromosome 21 open reading frame 33 | 1,4 | 1,8141 |
| ILMN_17715 | 6240 | RRM1 | ribonucleotide reductase M1 | 1,4 | 1,5007 |
| ILMN_32290 | 728310 | LOC728310 | golgin A6 family-like 7, pseudogene | 1,4 | 0,7969 |
| ILMN_17410 | 8396 | PIP4K2B | phosphatidylinositol-5-phosphate 4-kir | 1,4 | 1,0331 |
| ILMN_22916 | 117177 | RAB3IP | RAB3A interacting protein (rabin3) | 1,3 | 1,2499 |
| ILMN_17624 | 200895 | DHFRL1 | dihydrofolate reductase-like 1 | 1,3 | 2,6244 |
| ILMN_17340 | 338328 | GPIHBP1 | glycosylphosphatidylinositol anchored | 1,3 | 1,2499 |
| ILMN_21034 | 162967 | ZNF320 | zinc finger protein 320 | 1,3 | 0,3847 |
| ILMN_18041 | 222068 | TMED4 | transmembrane emp24 protein transp | 1,3 | 1,5007 |
| ILMN_17748 | 55591 | VEZT | vezatin, adherens junctions transmemb | 1,3 | 0,7969 |
| ILMN_17924 | 3267 | HRB | ArfGAP with FG repeats 1 | 1,3 | 1,8141 |
| ILMN_21814 | 147841 | SPC24 | SPC24, NDC80 kinetochore complex co | 1,3 | 0,7969 |
| ILMN_16765 | 10390 | CEPT1 | choline/ethanolamine phosphotransfe | 1,3 | 0,3847 |
| ILMN_17984 | 3218 | HOXB8 | homeobox B8 | 1,3 | 2,0799 |
| ILMN_23687 | 387522 | TMEM189-U | TMEM189-UBE2V1 readthrough | 1,3 | 2,0799 |
| ILMN_24012 | 10144 | FAM13A | family with sequence similarity 13, mer | 1,3 | 1,2499 |
| ILMN_16684 | 10350 | ABCA9 | ATP-binding cassette, sub-family A (AB | 1,3 | 0,7969 |
| ILMN_17710 | 2617 | GARS | glycyl-tRNA synthetase | 1,3 | 2,6244 |
| ILMN_17780 | 55066 | PDPR | pyruvate dehydrogenase phosphatase | 1,3 | 2,6244 |
| ILMN_32364 | 339736 | AK2P2 | adenylate kinase 2 pseudogene 2 | 1,3 | 0,7969 |
| ILMN_18057 | 389677 | RBM12B | RNA binding motif protein 12B | 1,3 | 0,7969 |
| ILMN_32396 | 84839 | RAX2 | retina and anterior neural fold homeob | 1,3 | 0,7969 |
| ILMN_21471 | 440348 | LOC440348 | nuclear pore complex interacting prote | 1,3 | 1,5007 |
| ILMN_17425 | 55149 | PAPD1 | mitochondrial poly(A) polymerase | 1,3 | 1,0331 |
| ILMN_20579 | 51101 | FAM164A | zinc finger, C2HC-type containing 1A | 1,3 | 0,3847 |
| ILMN_23680 | 6942 | TCF20 | transcription factor 20 (AR1) | 1,3 | 0,7969 |

| | | | | | |
|---|---|---|---|---|---|
| ILMN_17566 | 116115 | ZNF526 | zinc finger protein 526 | 1,3 | 2,6244 |
| ILMN_17910 | 51535 | PPHLN1 | periphilin 1 | 1,3 | 1,8141 |
| ILMN_17188 | 3225 | HOXC9 | homeobox C9 | 1,3 | 1,8141 |
| ILMN_17310 | 29896 | TRA2A | transformer 2 alpha homolog (Drosoph | 1,3 | 1,0331 |
| ILMN_24074 | 10922 | FASTK | Fas-activated serine/threonine kinase | 1,3 | 0,3847 |
| ILMN_33081 | 26834 | RNU4-2 | RNA, U4 small nuclear 2 | 1,3 | 2,6244 |
| ILMN_17140 | 57563 | KLHL8 | kelch-like 8 (Drosophila) | 1,3 | 0,7969 |
| ILMN_32386 | 692205 | SNORD89 | small nucleolar RNA, C/D box 89 | 1,3 | 1,2499 |
| ILMN_17196 | 9725 | TMEM63A | transmembrane protein 63A | 1,3 | 2,0799 |
| ILMN_17534 | 55095 | SAMD4B | sterile alpha motif domain containing 4 | 1,3 | 2,6244 |
| ILMN_22596 | 55904 | MLL5 | myeloid/lymphoid or mixed-lineage leu | 1,3 | 2,6244 |
| ILMN_17876 | 166647 | GPR125 | G protein-coupled receptor 125 | 1,3 | 1,0331 |
| ILMN_17481 | 1642 | DDB1 | damage-specific DNA binding protein 1 | 1,3 | 0,7969 |
| ILMN_16921 | 2768 | GNA12 | guanine nucleotide binding protein (G | 1,3 | 2,6244 |
| ILMN_17304 | 114793 | FMNL2 | formin-like 2 | 1,3 | 2,0799 |
| ILMN_17141 | 94241 | TP53INP1 | tumor protein p53 inducible nuclear pr | 1,3 | 0,6097 |
| ILMN_17333 | 83939 | EIF2A | eukaryotic translation initiation factor | 1,3 | 1,5007 |
| ILMN_17577 | 734 | OSGIN2 | oxidative stress induced growth inhibit | 1,3 | 2,6244 |
| ILMN_21750 | 6429 | SFRS4 | serine/arginine-rich splicing factor 4 | 1,3 | 2,6244 |
| ILMN_17247 | 8780 | RIOK3 | RIO kinase 3 (yeast) | 1,3 | 0,3847 |
| ILMN_17373 | 4000 | LMNA | lamin A/C | 1,3 | 1,5007 |
| ILMN_17656 | 10371 | SEMA3A | sema domain, immunoglobulin domain | 1,2 | 2,6244 |
| ILMN_23303 | 128387 | TATDN3 | TatD DNase domain containing 3 | 1,2 | 1,2499 |
| ILMN_17669 | 54988 | ACSM5 | acyl-CoA synthetase medium-chain fam | 1,2 | 1,2499 |
| ILMN_16768 | 9975 | NR1D2 | nuclear receptor subfamily 1, group D, | 1,2 | 2,0799 |
| ILMN_23228 | 51535 | PPHLN1 | periphilin 1 | 1,2 | 2,6244 |
| ILMN_16834 | 10452 | TOMM40 | translocase of outer mitochondrial mem | 1,2 | 1,5007 |
| ILMN_16914 | 83752 | LONP2 | lon peptidase 2, peroxisomal | 1,2 | 1,5007 |
| ILMN_32470 | 26781 | SNORA67 | small nucleolar RNA, H/ACA box 67 | 1,2 | 2,6244 |
| ILMN_16735 | 127428 | C1orf83 | transcription elongation factor A (SII) N | 1,2 | 2,0799 |
| ILMN_17760 | 165324 | UBXN2A | UBX domain protein 2A | 1,2 | 1,2499 |
| ILMN_21184 | 84293 | C10orf58 | family with sequence similarity 213, me | 1,2 | 0,3847 |
| ILMN_32419 | 246721 | POLR2J2 | polymerase (RNA) II (DNA directed) pol | 1,2 | 1,2499 |
| ILMN_32491 | 81566 | CSRNP2 | cysteine-serine-rich nuclear protein 2 | 1,2 | 1,5007 |
| ILMN_17927 | 1613 | DAPK3 | death-associated protein kinase 3 | 1,2 | 2,6244 |
| ILMN_16598 | 26472 | PPP1R14B | protein phosphatase 1, regulatory (inhi | 1,2 | 1,8141 |
| ILMN_17271 | 284390 | ZNF763 | zinc finger protein 763 | 1,2 | 0,3847 |
| ILMN_22909 | 9973 | CCS | copper chaperone for superoxide dism | 1,2 | 1,0331 |
| ILMN_21898 | 51077 | FCF1 | FCF1 small subunit (SSU) processome c | 1,2 | 2,0799 |
| ILMN_17687 | 81608 | FIP1L1 | FIP1 like 1 (S. cerevisiae) | 1,2 | 1,2499 |
| ILMN_23121 | 90338 | ZNF160 | zinc finger protein 160 | 1,2 | 0,3847 |
| ILMN_17102 | 79750 | ZNF385D | zinc finger protein 385D | 1,2 | 0,7969 |
| ILMN_17103 | 644591 | LOC644591 | peptidylprolyl isomerase A (cyclophilin | 1,2 | 0,3847 |
| ILMN_16827 | 8870 | IER3 | immediate early response 3 | 1,2 | 0,7969 |
| ILMN_21499 | 400511 | FLJ45256 | uncharacterized LOC400511 | 1,2 | 0,3847 |
| ILMN_16905 | 5533 | PPP3CC | protein phosphatase 3, catalytic subun | 1,2 | 1,0331 |

| | | | | | |
|---|---|---|---|---|---|
| ILMN_18151 | 400931 | FLJ27365 | MIRLET7B host gene (non-protein codi | 1,2 | 1,2499 |
| ILMN_17924 | 10109 | ARPC2 | actin related protein 2/3 complex, subu | 1,2 | 2,6244 |
| ILMN_17373 | 96459 | FNIP1 | folliculin interacting protein 1 | 1,2 | 1,8141 |
| ILMN_17116 | 6477 | SIAH1 | siah E3 ubiquitin protein ligase 1 | 1,2 | 0,7969 |
| ILMN_16954 | 5786 | PTPRA | protein tyrosine phosphatase, recepto | 1,2 | 1,0331 |
| ILMN_17634 | 23064 | SETX | senataxin | 1,2 | 0,3847 |
| ILMN_17246 | 29988 | SLC2A8 | solute carrier family 2 (facilitated gluco | 1,2 | 1,2499 |
| ILMN_22290 | 10201 | NME6 | NME/NM23 nucleoside diphosphate ki | 1,2 | 0,3847 |
| ILMN_16633 | 991 | CDC20 | cell division cycle 20 homolog (S. cerev | 1,2 | 1,8141 |
| ILMN_17194 | 4437 | MSH3 | mutS homolog 3 (E. coli) | 1,2 | 0,3847 |
| ILMN_16559 | 22936 | ELL2 | elongation factor, RNA polymerase II, 2 | 1,2 | 1,2499 |
| ILMN_17138 | 201895 | C4orf34 | chromosome 4 open reading frame 34 | 1,2 | 0,3847 |
| ILMN_17756 | 8672 | EIF4G3 | eukaryotic translation initiation factor | 1,2 | 1,2499 |
| ILMN_32489 | 619208 | C6orf225 | chromosome 6 open reading frame 22 | 1,2 | 1,5007 |
| ILMN_17227 | 9743 | RICS | Rho GTPase activating protein 32 | 1,2 | 1,5007 |
| ILMN_17726 | 23405 | DICER1 | dicer 1, ribonuclease type III | 1,2 | 1,0331 |
| ILMN_18009 | 5717 | PSMD11 | proteasome (prosome, macropain) 26S | 1,2 | 0,3847 |
| ILMN_17085 | 27125 | AFF4 | AF4/FMR2 family, member 4 | 1,2 | 2,0799 |
| ILMN_17755 | 1540 | CYLD | cylindromatosis (turban tumor syndror | 1,2 | 0,7969 |
| ILMN_22156 | 113457 | TUBA3D | tubulin, alpha 3d | 1,2 | 2,0799 |
| ILMN_22835 | 54463 | FAM134B | family with sequence similarity 134, me | 1,2 | 1,5007 |
| ILMN_17284 | 10565 | ARFGEF1 | ADP-ribosylation factor guanine nuclec | 1,2 | 0,7969 |
| ILMN_17011 | 9424 | KCNK6 | potassium channel, subfamily K, memb | 1,2 | 0,7969 |
| ILMN_17920 | 55596 | ZCCHC8 | zinc finger, CCHC domain containing 8 | 1,2 | 2,0799 |
| ILMN_16808 | 10046 | MAMLD1 | mastermind-like domain containing 1 | 1,2 | 0,3847 |
| ILMN_17787 | 51421 | AMOTL2 | angiomotin like 2 | 1,2 | 0,7969 |
| ILMN_17010 | 2055 | CLN8 | ceroid-lipofuscinosis, neuronal 8 (epile | 1,2 | 1,0331 |
| ILMN_20986 | 3995 | FADS3 | fatty acid desaturase 3 | 1,2 | 2,0799 |
| ILMN_32315 | 91584 | PLXNA4 | plexin A4 | 1,2 | 0,7969 |
| ILMN_17225 | 905 | CCNT2 | cyclin T2 | 1,1 | 2,0799 |
| ILMN_21971 | 55308 | DDX19A | DEAD (Asp-Glu-Ala-Asp) box polypeptic | 1,1 | 0,6097 |
| ILMN_16739 | 2969 | GTF2I | general transcription factor IIi | 1,1 | 2,0799 |
| ILMN_16616 | 401475 | SRRM1L | serine/arginine repetitive matrix 1 pseu | 1,1 | 1,5007 |
| ILMN_17431 | 23215 | BAT2D1 | proline-rich coiled-coil 2C | 1,1 | 2,0799 |
| ILMN_17912 | 85369 | FAM40A | family with sequence similarity 40, mer | 1,1 | 2,6244 |
| ILMN_17531 | 65125 | WNK1 | WNK lysine deficient protein kinase 1 | 1,1 | 2,6244 |
| ILMN_17827 | 90333 | ZNF468 | zinc finger protein 468 | 1,1 | 0,3847 |
| ILMN_17548 | 81545 | FBXO38 | F-box protein 38 | 1,1 | 1,0331 |
| ILMN_17429 | 7582 | ZNF33B | zinc finger protein 33B | 1,1 | 2,0799 |
| ILMN_17348 | 4524 | MTHFR | methylenetetrahydrofolate reductase ( | 1,1 | 1,0331 |
| ILMN_17929 | 4335 | MNT | MAX binding protein | 1,1 | 1,8141 |
| ILMN_17202 | 9320 | TRIP12 | thyroid hormone receptor interactor 1 | 1,1 | 2,6244 |
| ILMN_16685 | 11037 | STON1 | stonin 1 | 1,1 | 0,7969 |
| ILMN_17251 | 6905 | TBCE | tubulin folding cofactor E | 1,1 | 1,0331 |
| ILMN_16537 | 130617 | ZFAND2B | zinc finger, AN1-type domain 2B | 1,1 | 1,2499 |

)